

Design and Synthesis of Functionally Active 5-Amino-6-Aryl Pyrrolopyrimidine Inhibitors of Hematopoietic Progenitor Kinase 1

Rebecca A. Gallego,* Louise Bernier, Hui Chen, Sujin Cho-Schultz, Loanne Chung, Michael Collins, Matthew Del Bel, Jeff Elleraas, Cinthia Costa Jones, Ciaran N. Cronin, Martin Edwards, Xu Fang, Timothy Fisher, Mingying He, Jacqui Hoffman, Ruiduan Huo, Mehran Jalaie, Eric Johnson, Ted W. Johnson, Robert S. Kania, Manfred Kraus, Jennifer Lafontaine, Phuong Le, Tongnan Liu, Michael Maestre, Jean Matthews, Michele McTigue, Nichol Miller, Qiming Mu, Xulong Qin, Shijian Ren, Paul Richardson, Allison Rohner, Neal Sach, Li Shao, Graham Smith, Ruirui Su, Bin Sun, Sergei Timofeevski, Phuong Tran, Shuiwang Wang, Wei Wang, Ru Zhou, Jinjiang Zhu, and Sajiv K. Nair*



Cite This: *J. Med. Chem.* 2023, 66, 4888–4909



Read Online

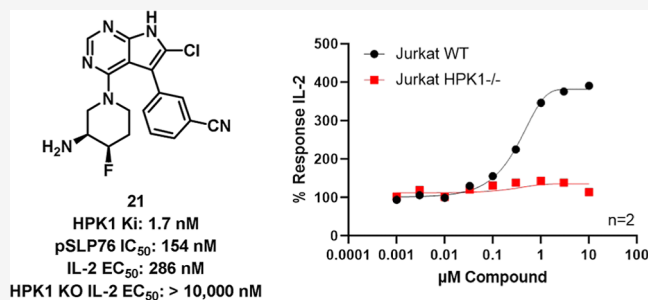
ACCESS |

Metrics & More

Article Recommendations

Supporting Information

ABSTRACT: Immune activating agents represent a valuable class of therapeutics for the treatment of cancer. An area of active research is expanding the types of these therapeutics that are available to patients via targeting new biological mechanisms. Hematopoietic progenitor kinase 1 (HPK1) is a negative regulator of immune signaling and a target of high interest for the treatment of cancer. Herein, we present the discovery and optimization of novel amino-6-aryl pyrrolopyrimidine inhibitors of HPK1 starting from hits identified via virtual screening. Key components of this discovery effort were structure-based drug design aided by analyses of normalized *B*-factors and optimization of lipophilic efficiency.



INTRODUCTION

Hematopoietic progenitor kinase 1 (HPK1), also known as mitogen-activated protein kinase kinase kinase 1 (MAP4K1), is a member of the mammalian Ste20-like family of serine/threonine kinases and a novel target for cancer immunotherapy.^{1–3} HPK1 acts proximal to the T cell receptor to dampen T cell receptor (TCR) activating signals.^{4–7} HPK1 knockout (KO) mice are viable and show enhanced immune function including elevated TCR signaling and cytokine production, enhanced dendritic cell (DC) maturation and function, increased susceptibility to experimental autoimmune encephalomyelitis and increased antibody production following immunization with keyhole limpet hemocyanin (KLH).^{8,9} Tumor growth studies in HPK1 KO mice showed more effective anti-tumor immunity than wildtype (WT) mice in a variety of tumor models.⁸ Kinase inactivation via mutation of the active site lysine of the kinase domain of HPK1 in mice enhanced TCR signaling and increased effector cytokine secretion.^{10,11} Combined PD-L1 blockade with HPK1 kinase inactivation improved anti-viral and anti-tumor immunity in vivo.¹¹

An early goal of our program was to develop a selective small-molecule HPK1 inhibitor suitable for evaluation of target inhibition in a cellular context. At the initiation of this work,

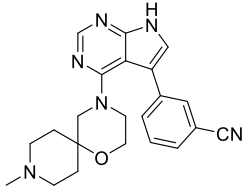
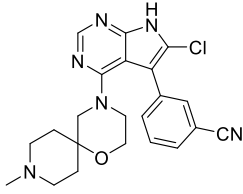
there were few literature-reported compounds with activity against HPK1;¹² however in recent years, there has been an explosion of research around the design of HPK1 inhibitors.¹³ Even with a large number of efforts in both academia and industry, an FDA-approved HPK1 inhibitor is yet to be realized. In the context of our efforts, exquisite selectivity was desired for achieving an HPK1-driven functional response in cell lines of interest, as there are many kinases involved in leukocyte signaling pathways which, if inhibited, result in immune suppression. Thus, to realize the full therapeutic potential of an HPK1 inhibitor, a successful clinical candidate would require high selectivity. Toward this goal, both biochemical and cell-based assays were used to assess selectivity. A cytokine production assay in both WT and HPK1 KO Jurkat cell lines reflected on-target HPK1 inhibition

Received: December 13, 2022

Published: March 20, 2023



Table 1. Initial Hit (Compound 1) and First-Generation Design Compound 2

Compound Number	Structure	HPK1 Biochemical Ki (LogD/LipE)	Jurkat pSLP76 cell IC ₅₀ (LipE)	Jurkat WT IL-2 cell IC ₅₀ /EC ₅₀ (max % response)	Jurkat HPK1 KO IL-2 cell IC ₅₀ /EC ₅₀ (max % response)	PKCθ Biochemical Ki (window) ^a	PKCη Biochemical Ki
1		17 ± 9 nM (1.4/6.4)	1,960 ± 121 nM (4.4)	IC ₅₀ = 323 ± 181 nM (28%)	IC ₅₀ = 259 ± 6 nM (15%)	22 ± 11 nM (1x)	2.4 ± 0.4 nM
2		2.9 ± 1.7 nM (2.0/6.5)	806 ± 105 nM (4.1)	IC ₅₀ = 1340 ± 148 nM (28%)	IC ₅₀ = 453 ± 279 nM (24%)	33 ± 14 nM (11x)	7.9 ± 0.6 nM

^aRelative to HPK1 K_i.

and selectivity against T cell signaling proteins. A peripheral blood mononuclear cell (PBMC) assay addressed cell health.

RESULTS AND DISCUSSION

Hit to Early Lead. Compound 1 (Table 1) was identified as a hit from virtual screening using LigandScout 4.2 and Glide to evaluate in-house kinome-directed compound sets in an HPK1 homology model since protein crystal structures were not yet available at the time of this work (Figure 1).

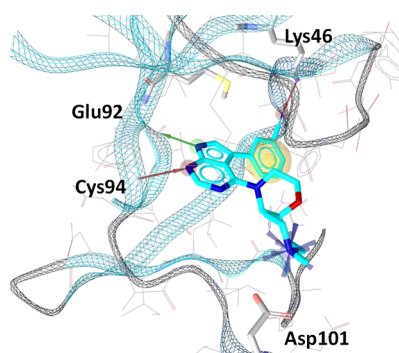


Figure 1. Compound 1 was identified by LigandScout as depicted here with the key pharmacophore highlighted: donor/acceptors pair at the hinge (Cys94/Glu92), a positively charged center interacting with Asp101, an acceptor feature capturing interactions to Lys46, and the excluded volume.

This compound was moderately selective, inhibiting 14 kinases >80% at 1 μM out of 70 tested. The HPK1 potency and selectivity made it desirable for follow up. Introduction of a chlorine atom adjacent to the gatekeeper residue increased potency without a change in lipophilic efficiency. As inhibition of HPK1 in the Jurkat cytokine production assay was expected to stimulate IL-2 production, the finding that both compound 1 and 2 showed dose-dependent decrease in IL-2 production

in WT and HPK1 KO Jurkat cells suggested that the selectivity profile was insufficient in these two early leads.

Analysis of selectivity data for a diverse panel of forty seven kinases, including some immune-relevant kinases involved in T-cell activation and signaling (e.g., LCK, FYN, PKCθ, IKK-β, and MAP4K4), showed that only four kinases were inhibited by both 1 and 2 >85% @ 1 μM inhibitor concentration (Figure 2 and Supporting Information). These kinases included PKCθ,

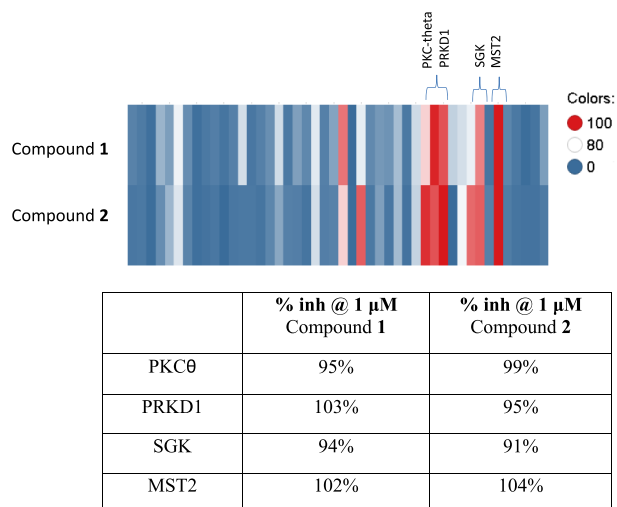


Figure 2. Invitrogen 1 μM inhibitor concentration % inhibition data for compounds 1 and 2.

PRKD1, SGK, and MST2. PKCθ is implicated in signal integration of the TCR and CD28 co-stimulatory pathways through activation of NFκB-mediated transcription and ultimately in the production of IL-2.¹⁴ Compounds 1 and 2 inhibited PKCθ at 95 and 99% @ 1 μM, respectively. This led to speculation that PKCθ inhibition caused functional effect

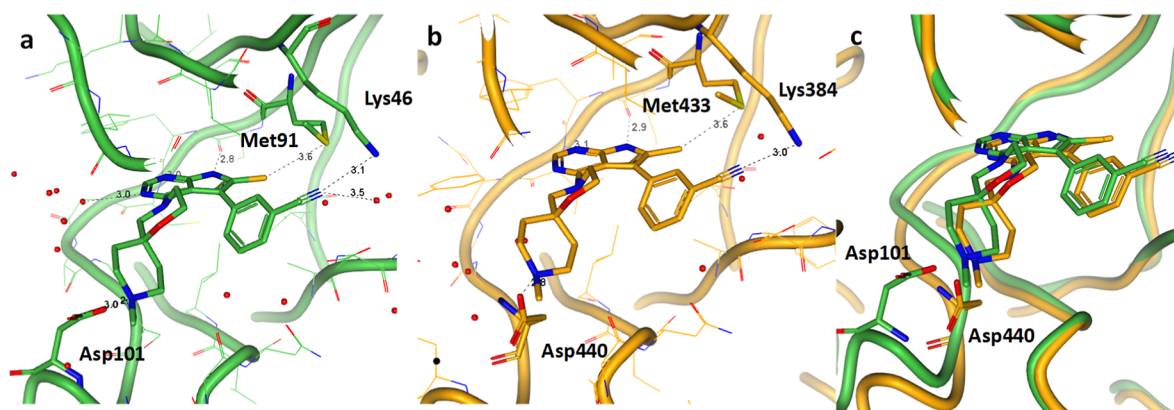


Figure 3. Co-crystal structures of compound **2** in (a) HPK1 T165E/S171E (1.83 Å, PDB 8FH4) (b) PKC η (1.75 Å, PDB 8FP1) (c) overlay of the structures in (a,b).

loss observed with compounds **1** and **2** in the IL-2 production assay.

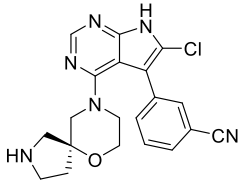
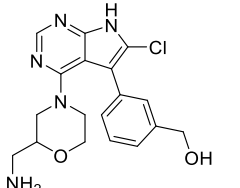
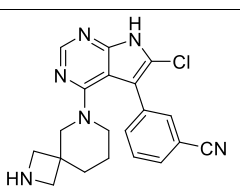
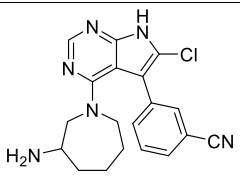
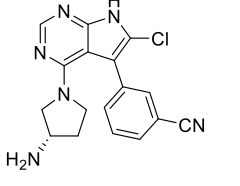
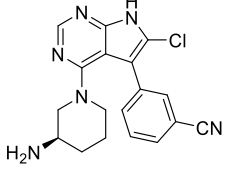
Improving Selectivity over PKC θ . Co-crystal structures were utilized to optimize potency and selectivity using structure-based drug design (SBDD).¹⁵ Structures of compound **2** in both HPK1 (PDB 8FH4) and PKC η (PDB 8FP1), a surrogate for PKC θ , were obtained (Figure 3). PKC η was identified as a viable surrogate to PKC θ based on the high homology between the two kinases and comparable biochemical activity for compounds of interest (Table 1). Compound **2** had a very similar binding mode in both HPK1 and PKC η . The chlorine atom at the C2 position on the ligand forms a close contact with the gatekeeper methionine in HPK1 (Met91) and PKC η (Met433). Similarly, in both complexes, the aryl nitrile interacts with the catalytic lysine at Lys46 and Lys384 for HPK1 and PKC η , respectively. Most significantly, the basic piperidine amine forms a salt bridge with Asp101 of HPK1. An efficient salt bridge can contribute 3.4 kcal/mol to binding energetics, which can translate to ca. 300-fold potency improvement relative to a protein that lacks this interaction. Although the PKC kinases lack an aspartic acid at that position (Met442), there is a proximal aspartic acid present at Asp440. The co-crystal structure of **2** in PKC η revealed a salt bridge interaction with this residue. Pliers scoring, an in-house MMGBSA score that reflects the summation of the electrostatics (ES), van der Waals (VdW), local ligand strain energy (LS) and the protein strain energy (PS), was completed for HPK1 and PKC η co-crystal structures with compound **2**. This showed that both complexes had low overall protein and ligand strain in the bound conformation (Supporting Information), which was consistent with the lack of selectivity seen for this compound.

The interaction with the aspartic acid at Asp101 in HPK1 was thought to contribute to the potency of **2** against HPK1, but the flexibility of the amine to pick up a salt bridge interaction at other positions likely contributed to undesired PKC θ activity. Given the hypothesized contribution of this salt bridge to potency against both targets, we speculated that optimization of the amine binding moiety to interact exclusively with Asp101 in HPK1 over other proximal aspartic acid residues (e.g. Asp440 in PKC η) would improve selectivity over the PKC family members as well as other kinases lacking an aspartic acid residue at this position, which accounts for approximately 68% of the kinome.

Designs were docked and scored (Pliers) in HPK1, and these conformations of the ligand in the bound state were evaluated in PKC η to assess the potential interaction with Asp440. The pyrrolidine spirocycle in compound **3** (Table 2) restricted conformational flexibility and more rigidly directed the amine toward Asp101 in HPK1 compared to Asp440 in the PKCs in modeling. While the HPK1 lipophilic efficiency (LipE)¹⁶ was improved over **2** (Table 1), the window over PKC θ was comparable (Table 2). A related acyclic version (**4**) had similar results, albeit with reduced efficiency for HPK1. A smaller azetidine spirocycle (**5**) also did not improve selectivity over PKC θ . Further decreasing the distance from the core to the amine (**6** and **7**) provided a minor improvement in the window over PKC θ , but with poor HPK1 potency and reduced efficiency relative to **2**. Maintaining a short linker to the amine (three heavy atoms from the core) but switching to a piperidine ring system (**8**), provided a potent HPK1 inhibitor (biochemical $K_i = 1.2$ nM, LipE = 7.1) with a large window for PKC θ (157-fold). The significant difference in the potency of the piperidine analogue relative to the pyrrolidine and azepane analogues was speculated to be related to the higher degree of freedom for rotation in the latter two. Modeling of compound **8** in HPK1 and subsequent crystal structures, described later herein, showed that the close spatial proximity of the piperidine and aryl nitrile groups may lock them in place and ideally orient the amine for interaction with Asp101 as well as the nitrile for interaction with Lys46. This illustrated the potential interplay between the groups extending from the core pyrrolopyrimidine. The potent biochemical activity of **8** translated to 491 nM pSLP76 IC₅₀ and 390 nM IL-2 EC₅₀ (272% max response) in WT Jurkat cells with minimal effect (EC₅₀ > 10 μ M) in HPK1 KO cells. This was a dramatic improvement relative to the initial hit (compound **1**), which by comparison, showed decreases in IL-2 production in both WT and KO cells upon compound treatment (Figure 4). This illustrated that selectivity over PKC θ was necessary to provide the desired functional response.

The directed amine interaction to Asp101 through a strong salt bridge was critical to obtaining HPK1 potency and aided in enhancing selectivity over PKC θ . The amine (**9**) and alcohol (**10**) pair of analogues showed that in the absence of the salt bridge interaction, HPK1 potency decreases by 9-fold along with a significant 2.6 unit decrease in lipophilic efficiency (Table 3). Further, selectivity over PKC θ for the alcohol eroded.

Table 2. Designs to Improve Selectivity over PKC θ

Compound Number	Structure	HPK1 Biochemical Ki (LogD/LipE)	Jurkat pSLP76 cell IC ₅₀ (LipE)	Jurkat WT IL-2 cell IC ₅₀ /EC ₅₀ (max % response)	Jurkat HPK1 KO IL-2 cell IC ₅₀ /EC ₅₀ (max % response)	PKC θ Biochemical Ki (window) ^a
3		18 ± 11 nM (0.73/7.0)	ND	ND	ND	24 ± 6 nM (1x)
4 ^b		95 ± 48 nM (0.80/6.2)	ND	ND	ND	90 ± 23 nM (1x)
5		37 ± 4 nM (0.61/6.8)	ND	ND	ND	63 ± 44 nM (2x)
6 ^b		112 ± 39 nM (1.1/5.8)	ND	ND	ND	>1,500 nM (>13x)
7		273 ± 227 nM (1.3/5.3)	ND	ND	ND	>1400 nM (>5x)
8		1.2 ± 0.6 nM (1.8/7.1)	419 ± 123 nM (4.6)	EC ₅₀ = 390 ± 187 nM (274%)	EC ₅₀ >10,000 nM (112%)	193 ± 105 nM (157x)

^aRelative to HPK1 K_i. ^bSingle enantiomer with unknown absolute stereochemistry. ^cn = 1.

Designing to Improve HPK1 Potency and Selectivity.

The glycine-rich loop (G-loop) region of the HPK1 binding pocket was targeted for additional increases in potency. HPK1 has a unique Gly24, Gly25, and Gly26 sequence that is only found in less than 2% of the kinome. The sequence of glycine residues was hypothesized to impart HPK1 with additional flexibility in this region that could accommodate steric bulk not tolerated in other kinases, thus allowing for an opportunity to improve broad kinase selectivity. Compound 11, with a methyl group oriented toward this region, provided a modest

improvement in potency and lipophilic efficiency in the biochemical and cellular assays, while improving the window over PKC θ to 258-fold (Table 4). Increasing the size of the methyl group to trifluoromethyl (12) did not increase potency relative to compound 11 and resulted in decreased efficiency. This could be a consequence of reduced pK_a of the basic amine and correspondingly decreased strength of the interaction to Asp101. The Moka pK_a values^{17–19} are 8.7 and 7.4 for compound 11 and 12, respectively. It is also possible that the

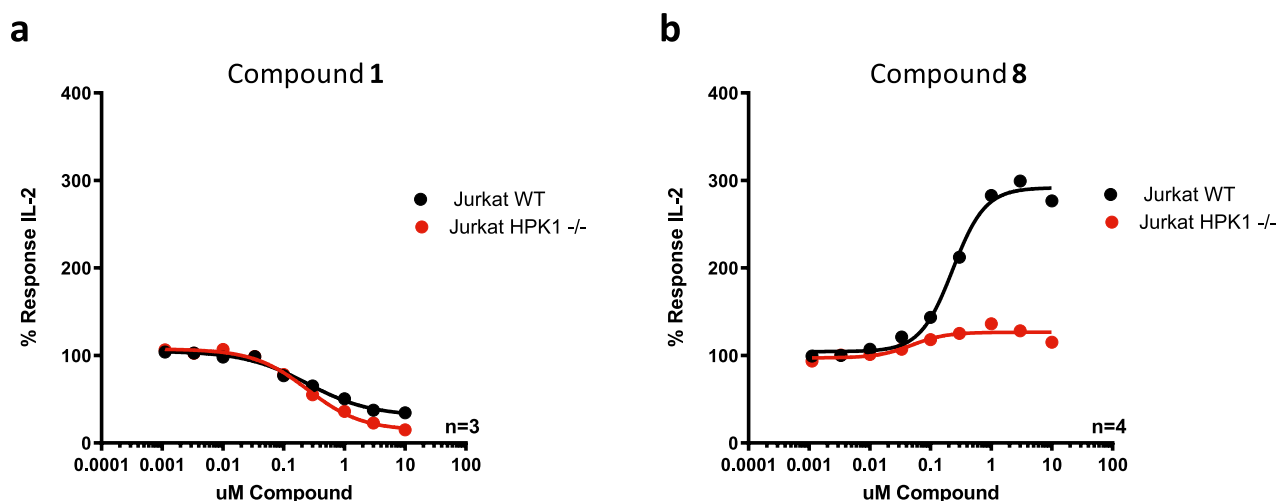


Figure 4. Jurkat IL-2 production assay in WT (black curve) and KO (red curve) cells for (a) compound 1 and (b) compound 8.

Table 3. Comparison of Basic and Neutral Matched Pairs

Compound Number	Structure	HPK1 Biochemical Ki (LogD/LipE)	Jurkat pSLP76 cell IC ₅₀ (LipE)	PKCθ Biochemical Ki (window) ^a
9		21 ± 13 nM (1.0/6.7)	1,430 ± 740 nM (4.8)	478 ± 162 nM (23x)
10		189 ± 93 nM (2.7/4.1)	>10,000 ^b (<2.4)	>1,200 nM (>6x)

^aRelative to HPK1 K_i. ^bn = 1.

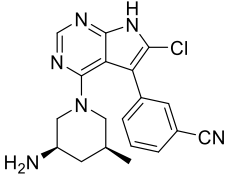
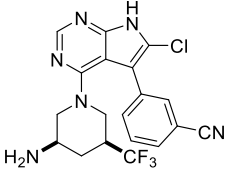
trifluoromethyl group in compound 12 is sterically too demanding for the HPK1 G-loop along that specific vector.

Based on the exquisite potency for HPK1 in biochemical and cellular assays, along with a significant window for selectivity over PKCθ, co-crystal structures of compound 11 in HPK1 (PDB 8FJZ) and PKCη (PDB 8FP3) were generated. While the structure in HPK1 showed an ideal distance (2.8 Å) for the interaction between the amine and Asp101 (Figure 5), the structure with PKCη showed an elongated bond distance (3.6 Å), indicating a non-ideal interaction. Furthermore, the G-loop in PKCη, which lacks the Gly24–26 sequence present in HPK1, resided higher above the inhibitor, possibly generating protein strain counter-productive to binding, whereas the carbonyl of Gly25 in HPK1 forms a close contact with the ligand.

Further optimization focused on the aryl head group. Removal of the nitrile (13) provided a decrease in efficiency for HPK1 (Table 5) compared to compound 11 (Table 4). Compound 14, which was designed to have a water-mediated interaction with the conserved lysine at Lys46, regained some efficiency in the biochemical assay relative to compound 13

but was much less active than compound 11. The benzylic alcohol (15) was prepared to determine whether interaction with the carbonyl group in Ala141, which is situated at the bottom of the ATP site, would provide additional potency/efficiency. While this compound was as potent and efficient as compound 11 in the biochemical assay, cellular activity and efficiency in the pSLP76 and IL-2 production assays were decreased. This may be driven by reduced permeability.²⁰ To improve potency without adding additional hydrogen bond donors that may affect permeability, the methyl (16), chloro (17), and fluoro phenyl nitrile (18) analogues were prepared in order to fill an apparent lipophilic pocket at the top of the ATP binding site. The methyl (16) and chloro (17) analogues were tested as an atropisomeric mixture, whereas the fluoro analogue (18) lacked atropisomerism, which was preferred since the aforementioned atropisomers interconverted at room temperature. Compound 18 represented a greater than five-fold increase in biochemical potency and 0.8 increase in LipE relative to 11. Compound 18 also provided an improvement in the pSLP76 and IL-2 production cellular assays. Compound 18, was a LipE winner in that it contained a small structural

Table 4. Designs to Improve HPK1 Potency via Targeting G-Loop (Gly24, Gly25, and Gly26) Region

Compound Number	Structure	HPK1 Biochemical Ki (LogD/LipE)	Jurkat pSLP76 cell IC ₅₀ (LipE)	Jurkat WT IL-2 cell IC ₅₀ /EC ₅₀ (max % response)	Jurkat HPK1 KO IL-2 cell IC ₅₀ /EC ₅₀ (max % response)	PKC θ Biochemical Ki (window) ^a
11		0.36 ± 0.10 nM (2.0/7.5)	140 ± 82 nM (4.9)	EC ₅₀ = 122 ± 60 nM (296%)	EC ₅₀ > 10,000 nM (129%)	93 ± 44 nM (258x)
12 ^b		0.59 ± 0.20 nM (3.0/6.2)	134 ± 33 nM (3.9)	EC ₅₀ = 177 ± 40 nM (301%)	EC ₅₀ = 318 ± 108 nM (242%)	116 ± 19 nM (197x)

^aRelative to HPK1 K_i. ^bSingle enantiomer with unknown absolute stereochemistry, cis relative stereochemistry.

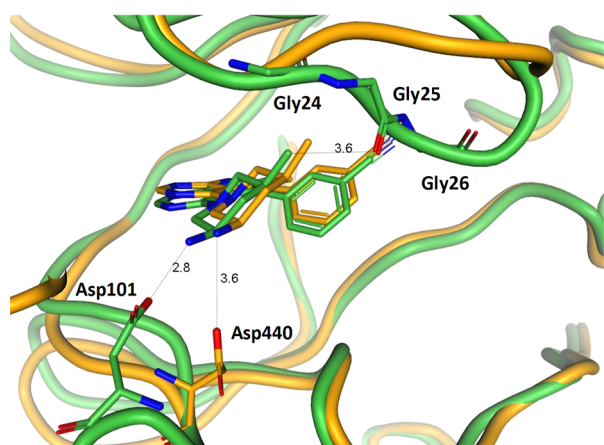


Figure 5. Co-crystal structures of compound **11** in HPK1 T165E/S171E (1.90 Å, PDB 8FJZ, green) and in PKC η (2.15 Å, PDB 8FP3, orange).

change that induced a significant increase in efficiency.¹⁶ In this case the increase in efficiency is driven by the increase in potency, which is thought to be due to the effect of filling a void in the binding pocket and also by altering the electronics of the adjacent nitrile, with no change in lipophilicity.

Improving Selectivity of Compound 18: MST1/2/3/4 and MAP4K2/3/5. Kinase selectivity data generated at Invitrogen showed that compound **18** inhibited only eight kinases with >90% at 0.1 μ M out of seventy-two tested (Figure 6 and Supporting Information). This was set as a threshold of interest because less than 90% inhibition predicted a greater than 100-fold biochemical selectivity window for HPK1 over the off-target when the percent inhibition value for the off-target was converted to a biochemical activity. The eight targets that compound **18** inhibited above that threshold included MAP4K2, MAP4K3, MAP4K5, MST4, MST1, MST2, TYK2, and MEK1.

While HPK1 Leu23 has branching at the C γ position of the side chain, and four out of the eight kinases inhibited by

compound **18** had a residue at this position with branching at the first atom (C β) on the sidechain (Figure 6). In next generation designs, steric bulk was extended toward Leu23 with the intent of clashing with C β -branched amino acids, but not with HPK1 (Table 6). Compound **19** introduced an axial methyl group on the piperidine ring to fill this vector. This analogue did not have reduced inhibition of MAP4K3, which was used as a sentinel kinase for the group of four key off-targets with C β -branched residues at this position, and lost approximately 270-fold potency for HPK1 in the biochemical assay relative to **11**.

To better design additional analogues using this strategy to improve selectivity, the structure–activity relationship for compounds **11** and **19** was further assessed. Both were modeled in an HPK1 co-crystal structure (PDB 8FJZ, obtained with compound **11**) and were scored using Pliers. This modeling showed a Pliers score of $\Delta\Delta G = 7.2$ for the two compounds, which correlated in direction and magnitude of the potency difference observed (Table 7). Of the various components of the Pliers score (ES, VdW, GS, SA, LS, and PS), the increased LS of compound **19** relative to compound **11** ($\Delta LS = 3.6$ kcal/mol) stood out as a potential contributor to the loss in potency.

Additionally, a co-crystal structure of HPK1 with compound **19** was obtained and was shown to be largely identical to the co-crystal structure with compound **11**, except for the position of Leu23, which was pushed back relative to the structure with **11** (Figure 7).

To determine if this movement in Leu23 was detrimental to binding through introduction of protein strain, an analysis of normalized B-factors (B') was also completed. This type of analysis has been reported in the literature to explain differences in potency for analogues of interest.^{21,22} The normalized B-factors for the residues of interest (Leu23–Val31) were obtained from the co-crystal structures of compounds **11** and **19**, and the difference was taken ($\Delta B'$). This was plotted relative to each atom on the residue (Figure 8). The threshold for a significant difference was set at 0.35

Table 5. 3-Substituted Aryl Groups to Improve HPK1 Potency

Compound Number	Structure	HPK1 Biochemical Ki (LogD/LipE)	Jurkat pSLP76 cell IC ₅₀ (LipE)	Jurkat WT IL-2 cell IC ₅₀ /EC ₅₀ (max % response)	Jurkat HPK1 KO IL-2 cell IC ₅₀ /EC ₅₀ (max % response)	PKC θ Biochemical Ki (window) ^a	RRCK P_{app} A to B ²⁰ (10 ⁻⁶ cm/s)
13		1.7 ± 0.6 nM (2.6/6.1)	362 ± 67 nM (3.8)	EC ₅₀ = 234 ± 57 nM (201%)	EC ₅₀ >10,000 nM (121%)	147 ± 38 nM (86x)	6.5
14		5.2 ± 3.2 nM (1.1/7.1)	1,080 ± 270 nM (4.8)	EC ₅₀ = 311 ± 55 nM (214%)	EC ₅₀ >10,000 nM (106%)	223 ± 46 nM (43x)	3.9
15		0.58 ± 0.30 nM (1.7/7.6)	316 ± 5.6 nM (4.8)	EC ₅₀ = 540 ± 384 nM (252%)	EC ₅₀ >10,000 nM (120%)	61 ± 20 nM (105x)	2.9
16		2.2 ± 1.4 nM (2.3/6.3)	473 ± 121 nM (4.0)	EC ₅₀ = 1,280 ± 487 nM (402%)	EC ₅₀ = 7,520 ± 4,280 nM (128%)	224 ± 74 nM (102x)	11
17		0.40 ± 0.27 nM ^b (2.4/7.0)	150 ± 31 nM (4.4)	EC ₅₀ = 335 ± 56 nM (337%)	EC ₅₀ = 7,000 ± 5,270 nM (118%)	74 ± 21 nM (185x)	11
18		<0.07 nM (2.0/8.3)	92 ± 28 nM (5.0)	EC ₅₀ = 42 ± 16 nM (239%)	EC ₅₀ >10,000 nM (90%)	23 ± 15 nM (>328x)	6.5

^aRelative to HPK1 K_i . ^b $n = 2$.

based on the median absolute deviation (MAD) of the $\Delta B'$ across the structure as a whole.²¹ This analysis showed that there was much more motion in the G-loop, particularly at Leu23, for the structure with compound **19** relative to the structure with compound **11**. This was consistent with a steric clash between the methyl group of compound **19** and Leu23 that induced protein strain and contributed to the decrease in potency of this compound for HPK1. Further, NMR studies with compound **19** showed that the strongly preferred solution state conformation positioned the amine to reside equatorially, which is the same conformation that was observed in the co-crystal structure with HPK1 (Supporting Information).

Together, normalized B-factor analysis and NMR studies of compound **19** indicated that steric clash with the protein was likely a major cause for the decrease in potency as opposed to other drivers predicted by the computational model, such as ligand strain. Next generation designs therefore focused on incorporation of subtler steric bulk oriented toward Leu23 from other vectors of the piperidine scaffold rather than reduction of ligand strain.

Fused pyrrolidine **20** (Table 6), which was designed to extend toward the outside of Leu23, had decreased potency against HPK1 relative to **11** and did not improve the MAP4K3 selectivity. Excitingly, increasing steric bulk toward the

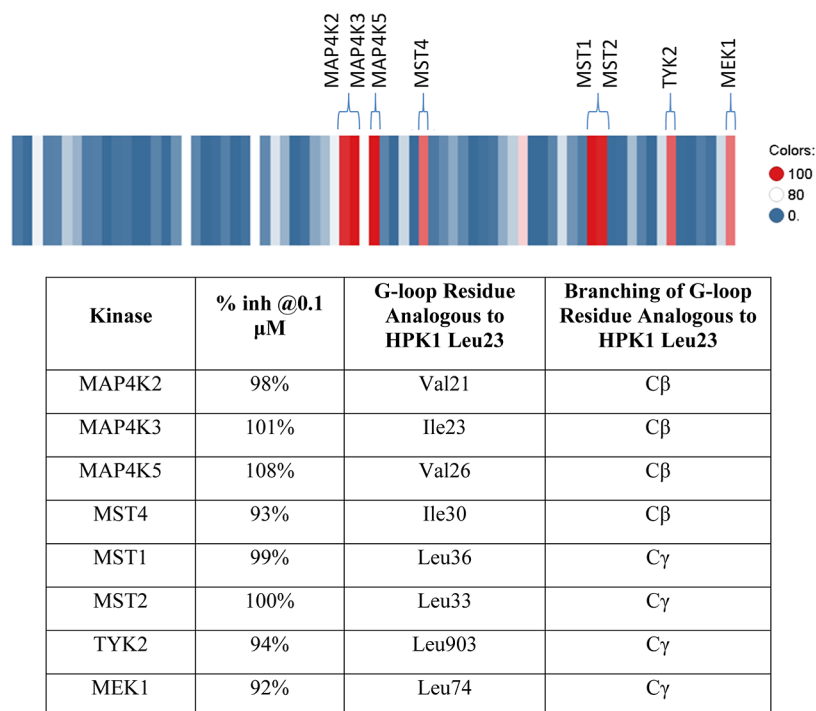


Figure 6. Invitrogen 0.1 μ M inhibitor concentration % inhibition data for compound 18.

Table 6. Design to Improve Selectivity against Kinases with C β Branching in the G-Loop

Compound Number	Structure	HPK1 Biochemical Ki (LogD/LipE)	Jurkat pSLP76 cell IC ₅₀ (LipE)	Jurkat WT IL-2 cell IC ₅₀ /EC ₅₀ (max % response)	Jurkat HPK1 KO IL-2 cell IC ₅₀ /EC ₅₀ (max % response)	MAP4K3 IC ₅₀ ^a (window) ^b
19		97 \pm 51 nM (1.6/5.4)	9,430 nM ^c (3.4)	ND	ND	110 nM \pm 33 nM (1x)
20		7.4 \pm 5.6 nM (1.3/6.8)	2,720 \pm 1710 nM (4.2)	EC ₅₀ = 864 \pm 1 nM (410%)	EC ₅₀ = 135 \pm 12 nM (201%)	7.0 \pm 5.0 nM (<1x)
21		1.7 \pm 0.5 nM (2.3/6.5)	154 \pm 70 nM (4.5)	EC ₅₀ = 286 \pm 88 nM (359%)	EC ₅₀ >10,000 nM (116%)	36 \pm 1 nM (21x)

^a $n = 2-3$. ^bRelative to HPK1 K_i. ^c $n = 1$.

backbone of Leu23 with a *cis*-fluoro substituted analogue (**21**) and improved the window over MAP4K3 to 21-fold and regained low nanomolar biochemical potency for HPK1 with

the same cellular LipE of the matched-pair des-fluoro analogue, compound **8**.

Table 7. Pliers Scoring of Compounds 11 and 19 in the Co-Crystal Structure of HPK1 T165E/S171E Crystallized with Compound 11

compound	ES ^a	VdW ^b	GB ^c	SA ^d	LS ^e	PS ^f	Pliers
11	-153.2	-41.8	139.3	-3.6	1.7	9.4	-48.2
19	-155.3	-41.5	144	-3.6	5.3	10.2	-41.0

^aElectrostatics. ^bvan der Waals. ^cGeneralized born solvation model. ^dSurface area contribution. ^eLigand strain. ^fProtein strain.

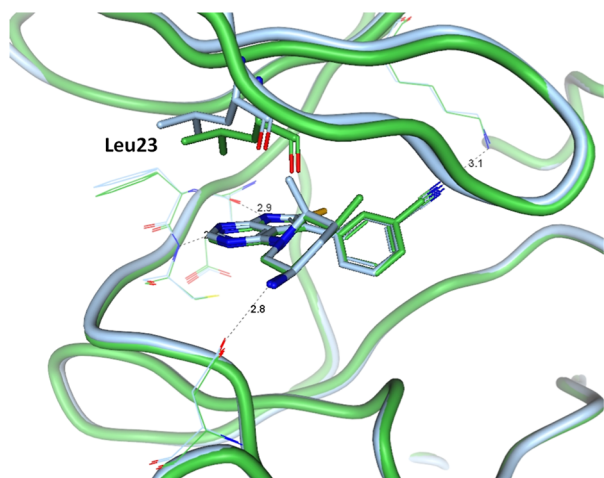


Figure 7. Co-crystal structures of compound 11 (green, 1.90 Å, PDB 8FJZ) and compound 19 in HPK1 T165E/S171E (blue, 2.10 Å, PDB 8FKO).

SYNTHETIC CHEMISTRY

The synthetic strategy for accessing the pyrrolopyrimidine inhibitors was designed to be modular, which allowed for late stage introduction of the most synthetically valuable component (Figure 9). From a general core intermediate (22), Suzuki cross-coupling could be used to introduce the C3

aryl group followed by nucleophilic aromatic substitution to bring in the C4 amine. This is referred to as a “right-to-left” sequence based on the order of functionalization as the compound is oriented when bound in the kinase hinge. Alternatively, a “left-to-right” sequence with sequential nucleophilic aromatic substitution and Suzuki cross-coupling reactions could be employed. Further, 22 could have the C2 functionality already installed, or it could be installed in a late stage manner from 25, if advantageous.

The synthesis of compound 11 illustrates the “right-to-left” approach. Compound 26, which was prepared using a known route,²³ was chlorinated using lithium hexamethyldisilazide and hexachloroethane to give 27 in 84% yield (Figure 10). This provided a tri-halogenated core that could be efficiently leveraged for diverse analogue synthesis. A sequence of Suzuki cross-coupling, nucleophilic aromatic substitution, and protecting group cleavage sequence provided compound 11. This route efficiently furnished a number of analogues using commercially available aryl boronic acids and amines (2, 16, 18, 20, and 21).

The “left-to-right” strategy was used to access 19 (Figure 11). The fully functionalized tri-halogenated core (27) underwent nucleophilic aromatic substitution with the requisite *cis*-piperidine amine²⁴ to access 30 in 71% yield. Suzuki cross-coupling and deprotection yielded the final analogue (19). This “left-to-right” approach was important in providing access to this analogue because the “right-to-left”

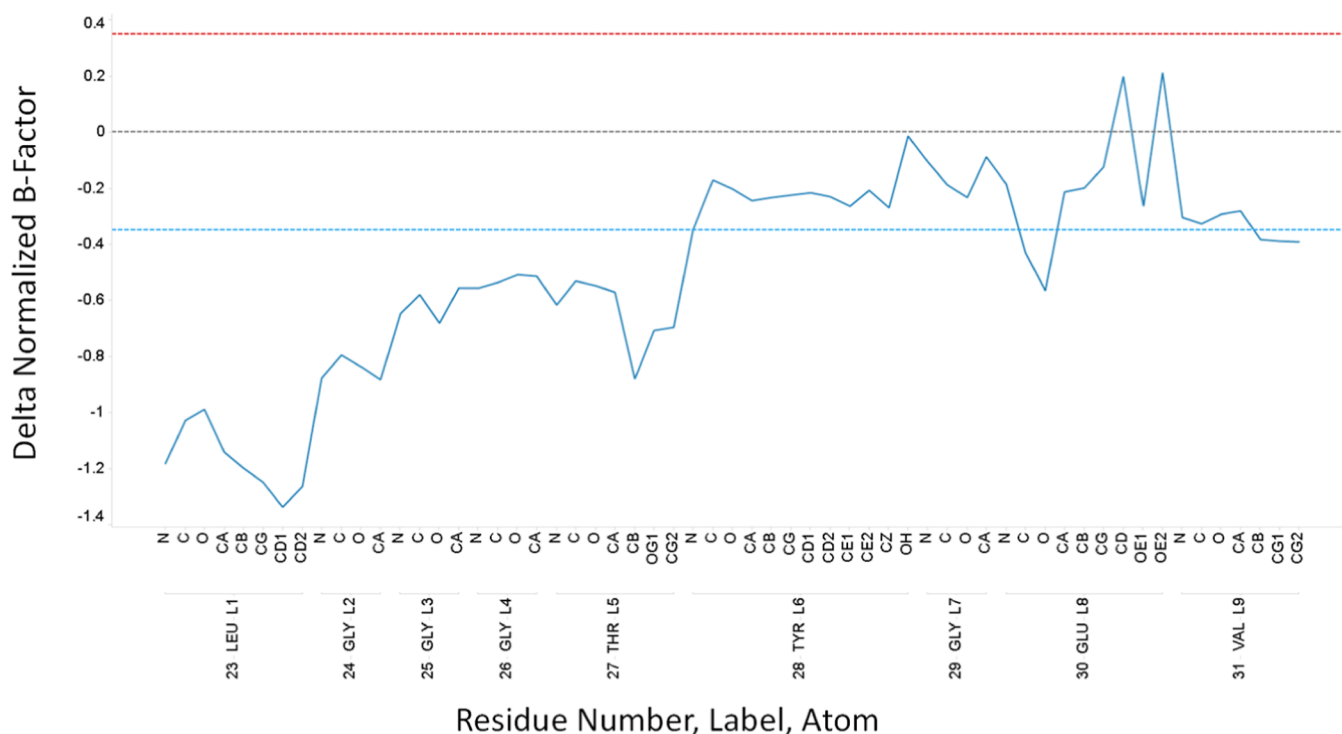


Figure 8. Plot of normalized *B*-factors differential for HPK1 co-crystal structures with compounds 11 and 19.

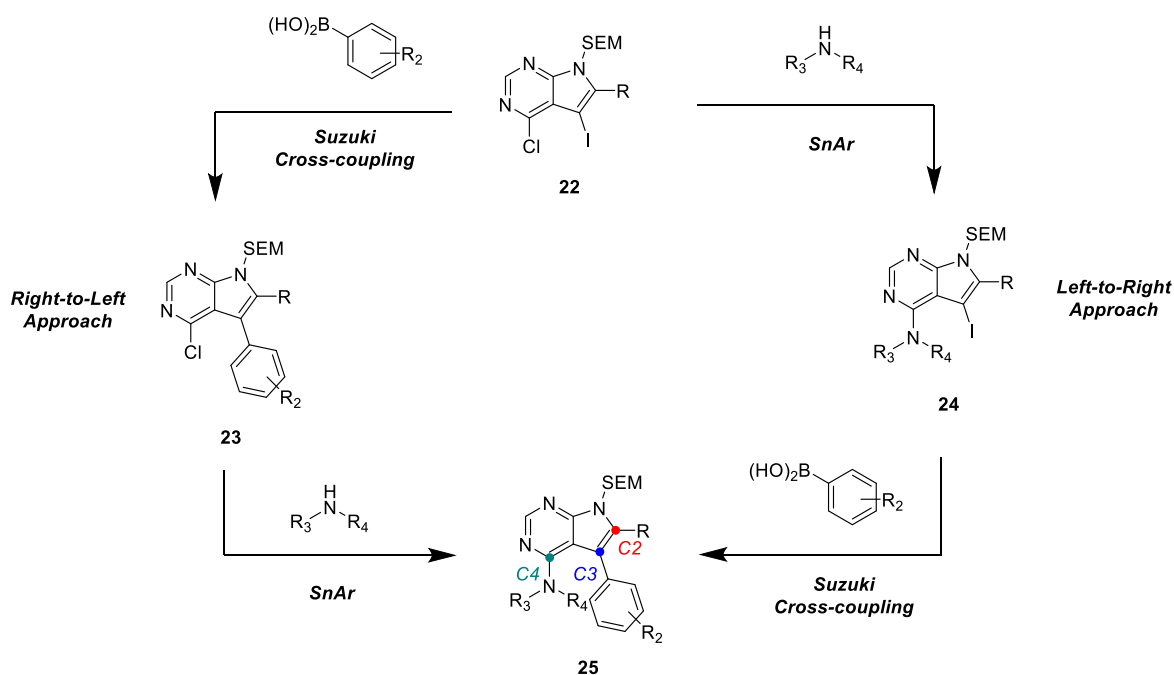


Figure 9. General synthetic strategy to access pyrrolopyrimidine inhibitors in a modular fashion.

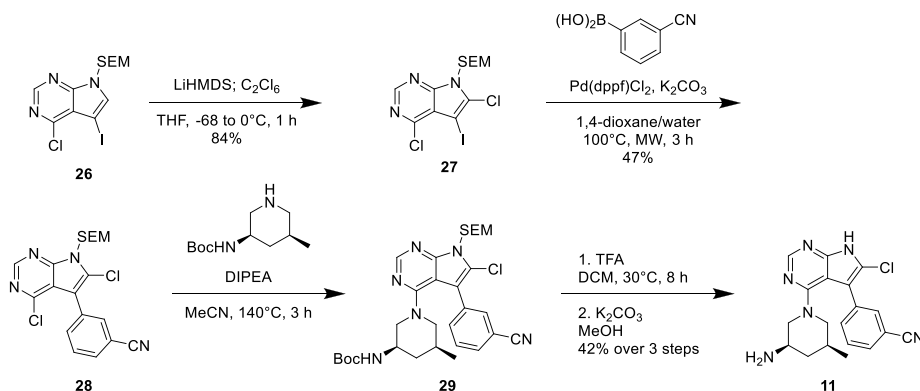


Figure 10. Synthesis of compound 11 using a “right to left” approach via sequential Suzuki cross-coupling and nucleophilic aromatic substitution reactions. Compounds 2, 8, 16, 18, 20, and 21 were synthesized using the same route.

strategy failed, presumably due to steric hindrance of the system. This route was also effective in providing a number of diverse analogues (5, 6, 7, 12, 13, 14, and 17).

A pyridine reduction strategy was employed to access non-commercially available *cis*-disubstituted piperidines, such as 34 (Figure 12).²⁵ Protection of aminopyridine (32) provided the *bis*-Boc protected substrate (33). Hydrogenation conditions successively cleaved one of the Boc protecting groups and hydrogenated the pyridine to provide the desired racemic amine (34).

CONCLUSIONS

Utilizing SBDD, a hit from compound screening which lacked the expected functional response was optimized to provide potent HPK1 inhibitors, such as compound 21, with the appropriate phenotype in a cytokine production assay which met the goal of this work. These inhibitors were suitable to evaluate the selective inhibition of HPK1 in a cellular context and could form the starting points for additional optimization to deliver a clinical candidate. Key challenges solved included improving HPK1 potency by over 200-fold, dramatically

increasing the selectivity over PKC θ from less than 20-fold to over 300-fold and additionally improving the selectivity over MAP4K3, a kinase with high homology to HPK1, from nonselective to 21-fold. Valuable tools used during this optimization include SBDD which leveraged co-crystal structures of key compounds in HPK1 and PKC η as well as normalized *B*-factor analysis. Efficient synthetic methods utilizing a modular, late-stage diversification strategy were developed in order to ensure rapid access to analogues in this series. A future publication will disclose the delivery of HPK1 inhibitors that were optimized for use in vivo.

EXPERIMENTAL SECTION

Starting materials and other reagents were purchased from commercial suppliers and were used without further purification unless otherwise indicated. All reactions were performed under a positive pressure of nitrogen or argon gas in anhydrous solvents (unless otherwise indicated). Reactions run at ambient temperature were between 15 and 30 °C. Analytical thin-layer chromatography was performed on glass-backed silica gel 60 F 254 plates [Analtech (0.25 mm)] and eluted with appropriate solvent ratios (v/v). The reactions were assayed with high-performance liquid chromatography

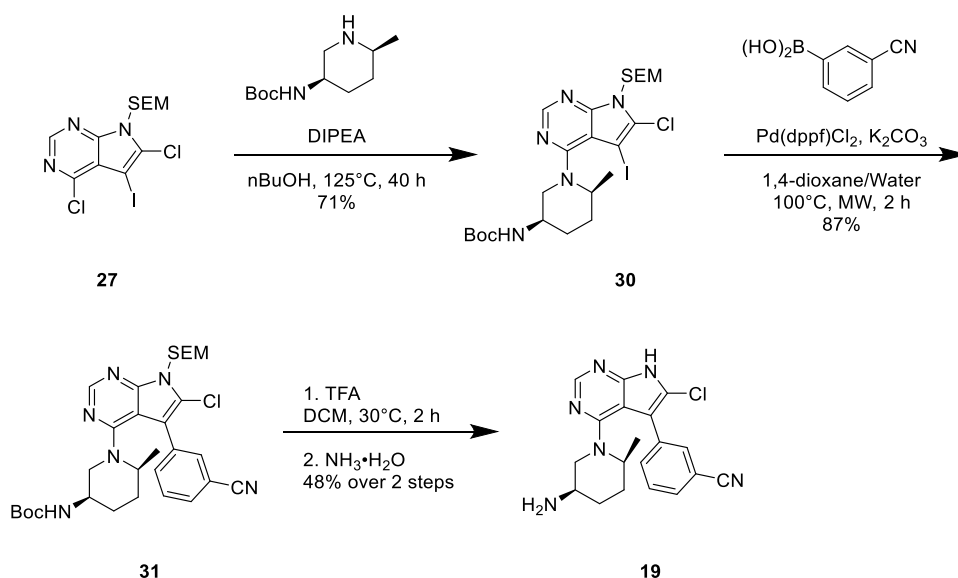


Figure 11. Synthesis of compound 19 using a “right to left” approach via sequential nucleophilic aromatic substitution and Suzuki cross-coupling reactions. Compounds 5, 6, 7, 12, 13, 14, and 17 were synthesized using the same route.

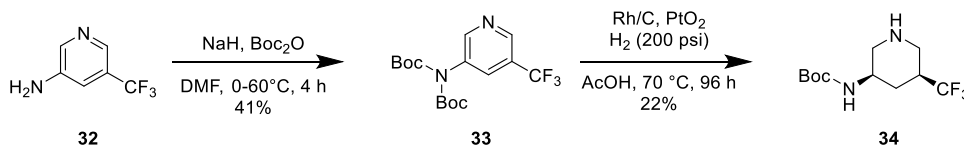


Figure 12. Synthesis of *cis*-piperidine 34.

(HPLC) or thin-layer chromatography (TLC) and terminated as judged by the composition of starting material. TLC plates were visualized by UV (254 nm). Microwave-assisted reactions were run in a Biotage initiator. ^1H NMR spectra were recorded on a Bruker instrument operating at 400 MHz unless otherwise indicated. ^1H NMR spectra are reported as obtained in DMSO- d_6 , D_2O , methanol- d_4 , or CDCl_3 solutions as indicated (reported in parts per million) using DMSO (2.54 ppm), water (4.60 ppm), methanol (3.34 ppm) or chloroform (7.26 ppm) as the reference standards, respectively.²⁶ When peak multiplicities are reported, the following abbreviations are used: s = singlet, d = doublet, t = triplet, br = broad. Coupling constants, when given, are reported in hertz. The mass spectra were obtained using liquid chromatography–mass spectrometry (LCMS) on an Agilent instrument using atmospheric pressure chemical ionization (APCI) or electrospray ionization (ESI). (*) denotes a center that depicts a single enantiomer with absolute stereochemistry unknown. LCMS and HPLC were used to determine purity of analogues generated for biological testing. Purity of lead compounds was determined to be >95% unless otherwise noted. Compounds 3, 4, and 5 were determined to be 89, 93 and 94% pure by HPLC.

tert-Butyl ((3*R*)-1-[5-(3-Cyanophenyl)-7-[[2-(trimethylsilyl)ethoxy]methyl]-7*H*-pyrrolo[2,3-*d*]pyrimidin-4-yl]piperidin-3-yl)carbamate (S1). A flask was charged with 3-(4-chloro-7-[[2-(trimethylsilyl)ethoxy]methyl]-7*H*-pyrrolo[2,3-*d*]pyrimidin-5-yl)-benzonitrile²³ (150 mg, 0.390 mmol), *tert*-butyl (3*R*)-piperidin-3-ylcarbamate (117 mg, 0.585 mmol), DIPEA (201 mg, 1.56 mmol), and DMSO (6 mL). The mixture was sealed and heated to 100 °C for 12 h. The reaction was cooled to room temperature and diluted with ethyl acetate (20 mL) and water (10 mL). The layers were separated, and the aqueous layer was extracted with ethyl acetate (3 × 25 mL). The combine organic layer was washed with brine (3 × 25 mL), dried over anhydrous sodium sulfate, filtered, and concentrated to provide the title compound as a yellow gum (200 mg, 94%). This material was brought on to the next step without further purification.

3-[4-((3*R*)-3-Aminopiperidin-1-yl)-7*H*-pyrrolo[2,3-*d*]pyrimidin-5-yl]benzonitrile (9). A flask was charged with *tert*-butyl

{(3*R*)-1-[5-(3-cyanophenyl)-7-[[2-(trimethylsilyl)ethoxy]methyl]-7*H*-pyrrolo[2,3-*d*]pyrimidin-4-yl]piperidin-3-yl}carbamate S1 (200 mg, 0.364 mmol) and DCM (4 mL). Trifluoroacetic acid (4 mL) was added, and the reaction was allowed to stir at 25 °C for 2 h. The mixture was concentrated in vacuo, and 1,4-dioxane (3 mL) and 28% aqueous ammonium hydroxide (1 mL) were added to the resulting residue. The mixture was allowed to stir at 20 °C for 2 h, and the solution was concentrated in vacuo to provide a yellow gum. The crude material was purified using preparative HPLC (0–30% acetonitrile in 0.2% aqueous formic acid, gradient time = 10 min, flow rate = 30 mL/min, Daiso C. Ltd. Daisogel C18, 150 mm × 25 mm × 5 μm column) to provide the title compound (18.5 mg, 15%). LC–MS (ESI) m/z : 318.9 ($M + H$)⁺; ^1H NMR (400 MHz, methanol- d_4): δ 8.42 (s, 1H), 7.90 (s, 1H), 7.85 (d, $J = 7.5$ Hz, 1H), 7.71–7.60 (m, 2H), 7.50 (s, 1H), 4.23 (d, $J = 9.0$ Hz, 1H), 3.45–3.35 (m, 2H), 3.15 (dd, $J = 9.7, 12.7$ Hz, 1H), 2.78–2.67 (m, 1H), 2.10–1.99 (m, 1H), 1.57–1.41 (m, 2H), 1.31–1.15 (m, 1H).

3-[4-(9-Methyl-1-oxa-4,9-diazaspiro[5.5]undec-4-yl)-7-[[2-(trimethylsilyl)ethoxy]methyl]-7*H*-pyrrolo[2,3-*d*]pyrimidin-5-yl]benzonitrile (S2). A flask was charged with 3-(4-chloro-7-[[2-(trimethylsilyl)ethoxy]methyl]-7*H*-pyrrolo[2,3-*d*]pyrimidin-5-yl)-benzonitrile²³ (600 mg, 1.56 mmol), 9-methyl-1-oxa-4,9-diazaspiro[5.5]undecane (483 mg, 2.34 mmol), DIPEA (806 mg, 6.23 mmol), and DMSO (5 mL). The reaction was sealed and heated to 100 °C for 12 h, at which point the reaction was judged to be complete by LCMS. The reaction was diluted with ethyl acetate (20 mL) and water (10 mL). The organic layer was separated and washed with water (3 × 10 mL). The combined aqueous layer was extracted with ethyl acetate (2 × 10 mL). The combined organic layer was washed with brine (3 × 10 mL), dried over anhydrous sodium sulfate, filtered, and concentrated. The crude material was purified using column chromatography (10:1 DCM/methanol) to provide the title compound as a yellow oil (600 mg, 74%). LC–MS (ESI) m/z : 519.1 ($M + H$)⁺; ^1H NMR (400 MHz, CDCl_3): δ 8.53 (s, 1H), 7.84 (s, 1H), 7.76 (d, $J = 8.0$ Hz, 1H), 7.63 (d, $J = 8.0$ Hz, 1H), 7.57–7.55 (m, 1H), 7.28 (s, 1H), 5.66 (s, 2H), 3.62–3.58 (m, 2H), 3.37–3.35

(m, 2H), 3.28 (s, 2H), 3.15–3.13 (m, 2H), 2.59 (br s, 2H), 2.34–2.33 (m, 5H), 1.96–1.93 (m, 2H), 1.69 (br s, 2H), 0.95 (t, $J = 8.4$ Hz, 2H), 0.01 (s, 9H).

3-[4-(9-Methyl-1-oxa-4,9-diazaspiro[5.5]undec-4-yl)-7H-pyrrolo[2,3-d]pyrimidin-5-yl]benzoxazole (1). A flask was charged with 3-[4-(9-methyl-1-oxa-4,9-diazaspiro[5.5]undec-4-yl)-7-[[2-(trimethylsilyl)ethoxy]methyl]-7H-pyrrolo[2,3-d]pyrimidin-5-yl]benzoxazole **S2** (600 mg, 1.16 mmol) and DCM (10 mL). Trifluoroacetic acid (10 mL) was added, and the solution was allowed to stir at 20 °C for 1 h, at which point the reaction was judged to be complete by LCMS. The mixture was concentrated in vacuo with the addition of DCM (3 × 20 mL). The resulting material was dissolved in 1,4-dioxane (4 mL) and 28% aqueous ammonium hydroxide (2 mL). The reaction was stirred at 20 °C for 1 h and then concentrated in vacuo. The crude product was purified using HPLC (0–30% acetonitrile in 0.2% aqueous formic acid, gradient time = 10 min, flow rate = 50 mL/min, Phenomenex Gemini C18 250 mm × 50 mm × 10 μm column) to provide the title compound as a white solid (155 mg, 34%). LC–MS (ESI) m/z : 389.0 (M + H)⁺; ¹H NMR (400 MHz, D₂O): δ 8.42–8.33 (m, 1H), 8.23–8.18 (m, 1H), 7.60–7.53 (m, 2H), 7.50–7.43 (m, 1H), 7.17–7.07 (m, 2H), 3.39–3.28 (m, 2H), 3.18–3.05 (m, 6H), 2.82 (s, 3H), 2.76–2.69 (m, 2H), 2.22–2.07 (m, 2H), 1.79–1.64 (m, 2H).

4,6-Dichloro-5-iodo-7-[[2-(trimethylsilyl)ethoxy]methyl]-7H-pyrrolo[2,3-d]pyrimidine (27). A flask was charged with 4-chloro-5-iodo-7-[[2-(trimethylsilyl)ethoxy]methyl]-7H-pyrrolo[2,3-d]pyrimidine **26**²³ (59.0 g, 144 mmol) and THF (680 mL) and was cooled to –78 °C under a nitrogen atmosphere. A 1 M solution of LiHMDS in THF (202 mL, 202 mmol) was added dropwise, and the reaction was allowed to stir for 1 h, at which point a pale white suspension was formed. A solution of hexachloroethane (51.1 g, 216 mmol) was added in THF (220 mL) dropwise. The reaction was allowed to warm to 0 °C and stirred for an additional hour at that temperature. An aqueous solution of saturated ammonium chloride (480 mL) was added. The mixture was combined with another batch of material from a 65 g scale reaction. The layers were separated, and the aqueous layer was extracted with ethyl acetate (2 × 500 mL). The combined organic layer was washed with brine (2 × 100 mL), dried over anhydrous sodium sulfate, filtered, and concentrated to provide a yellow gum (180 g). The combined material was dissolved in DCM (200 mL) and then diluted with petroleum ether (800 mL). The DCM was removed in vacuo until most of the solid material had precipitated. The suspension was stirred at 0 °C for 0.5 h and then was filtered. The filter cake was washed with petroleum ether (2 × 50 mL), and the solid was dried under house vacuum to provide the title compound as a light-yellow solid (113 g, average yield 84%). LC–MS (ESI) m/z : 443.9 (M + H)⁺; ¹H NMR (400 MHz, CDCl₃): δ 8.66 (s, 1H), 5.81–5.72 (m, 2H), 3.65–3.56 (m, 2H), 0.99–0.89 (m, 2H), 0.01–0.06 (m, 9H).

3-(4,6-Dichloro-7-[[2-(trimethylsilyl)ethoxy]methyl]-7H-pyrrolo[2,3-d]pyrimidin-5-yl)benzoxazole (28). A microwave vial was charged with 4,6-dichloro-5-iodo-7-[[2-(trimethylsilyl)ethoxy]methyl]-7H-pyrrolo[2,3-d]pyrimidine **27** (500 mg, 1.13 mmol) and water (2.5 mL) and 1,4-dioxane (10 mL). Under a nitrogen atmosphere, (3-cyanophenyl)boronic acid (182 mg, 1.24 mmol) was added followed by potassium carbonate (311 mg, 2.25 mmol) and [1,1'-bis(diphenylphosphino)ferrocene]dichloropalladium(II) (57.5 mg, 0.078 mmol). The solution was bubbled with nitrogen gas for 10 min and then stirred at 100 °C in a microwave for 3 h. The reaction was cooled and diluted with ethyl acetate (100 mL). The mixture was washed with brine (30 mL), dried over anhydrous sodium sulfate, filtered, and concentrated to provide a yellow oil (600 mg). The crude material was purified using column chromatography (5:1 petroleum ether/ethyl acetate) to provide the title compound as a yellow oil (220 mg, 47%). LC–MS (ESI) m/z : 419.1 (M + H)⁺; ¹H NMR (400 MHz, CDCl₃): δ 8.71 (s, 1H), 7.79 (t, $J = 1.4$ Hz, 1H), 7.75–7.69 (m, 2H), 7.63–7.56 (m, 1H), 5.80 (s, 2H), 3.72–3.63 (m, 2H), 1.03–0.92 (m, 2H), –0.02 (s, 9H).

tert-Butyl 9-[6-Chloro-5-(3-cyanophenyl)-7-[[2-(trimethylsilyl)ethoxy]methyl]-7H-pyrrolo[2,3-d]pyrimidin-4-

yl]-6-oxa-2,9-diazaspiro[4.5]decane-2-carboxylate (S3). A microwave vial was charged with 3-(4,6-dichloro-7-[[2-(trimethylsilyl)ethoxy]methyl]-7H-pyrrolo[2,3-d]pyrimidin-5-yl)benzoxazole **28** (213 mg, 0.508 mmol), *tert*-butyl 6-oxa-2,9-diazaspiro[4.5]decane-2-carboxylate (119 mg, 0.572 mmol), DIPEA (0.4 mL, 2.54 mmol), and acetonitrile (2.4 mL). The reaction was heated to 100 °C in a microwave for 2 h and then to 120 °C in a microwave for 8 h. The mixture was concentrated in vacuo and purified using column chromatography (0–100% ethyl acetate in heptane) to provide the title compound as a pale-yellow foam (312 mg, 98%). LC–MS (APCI) m/z : 626.2 (M + H)⁺; ¹H NMR (400 MHz, CDCl₃): δ 8.55 (s, 1H), 7.85 (s, 1H), 7.60–7.75 (m, 3H), 5.77 (s, 2H), 3.67–3.81 (m, 2H), 3.32–3.56 (m, 6H), 3.08–3.27 (m, 2H), 2.95–3.16 (m, 2H), 1.81–1.95 (m, 1H), 1.49 (s, 9H), 0.91–1.08 (m, 2H), 0.03 (s, 9H).

3-[6-Chloro-4-[(5S)-6-oxa-2,9-diazaspiro[4.5]dec-9-yl]-7H-pyrrolo[2,3-d]pyrimidin-5-yl]benzoxazole (3). To a stirred solution of *tert*-butyl 9-[6-chloro-5-(3-cyanophenyl)-7-[[2-(trimethylsilyl)ethoxy]methyl]-7H-pyrrolo[2,3-d]pyrimidin-4-yl]-6-oxa-2,9-diazaspiro[4.5]decane-2-carboxylate **S3** (312 mg, 0.499 mmol) in DCM (3 mL) was added trifluoroacetic acid (1 mL). The reaction was allowed to stir at room temperature for 16 h. The mixture was concentrated in vacuo and azeotroped with toluene (3×). The resulting material was dissolved in methanol (3 mL) and 7 N ammonia in methanol (3 mL) and stirred at room temperature for 4 h. The reaction was concentrated in vacuo and azeotroped with toluene (3×). The material was purified, and the enantiomers were separated using SFC (50% methanol + 10 mM ammonia in carbon dioxide with pressure at 120 bar, flow rate = 4 mL/min, Phenomenex Lux Cellulose-2 4.6 mm × 250 mm × 5 μm column, peak 2). This provided the title compound as a solid (57.0 mg, 28%). LC–MS (APCI) m/z : 395.1 (M + H)⁺; ¹H NMR (400 MHz, DMSO-*d*₆): δ 8.36 (s, 1H), 7.75–7.91 (m, 3H), 7.60–7.73 (m, 1H), 3.03–3.20 (m, 4H), 2.78–2.92 (m, 6H), 1.62–1.88 (m, 2H).

[3-(4-Chloro-7-[[2-(trimethylsilyl)ethoxy]methyl]-7H-pyrrolo[2,3-d]pyrimidin-5-yl)phenyl]methanol (S4). A flask was charged with 4-chloro-5-iodo-7-[[2-(trimethylsilyl)ethoxy]methyl]-7H-pyrrolo[2,3-d]pyrimidine **26**²³ (6.60 g, 16.1 mmol), [3-(hydroxymethyl)phenyl]boronic acid (2.94 g, 19.3 mmol), [1,1'-bis(diphenylphosphino)ferrocene]dichloropalladium(II) (589 mg, 0.805 mmol), cesium carbonate (15.7 g, 48.3 mmol), 1,4-dioxane (104 mL), and water (26 mL). The reaction mixture was heated to 70 °C under a nitrogen atmosphere for 16 h. TLC (3:1 petroleum ether/ethyl acetate, UV visualization) showed consumption of the starting material. The reaction mixture was diluted with water (100 mL) and extracted with ethyl acetate (3 × 150 mL). The combined organic layer was washed with brine (3 × 100 mL), dried over sodium sulfate, filtered, and concentrated. The crude product was purified using column chromatography (3:1 petroleum ether/ethyl acetate) to provide the title compound as a yellow solid (4.2 g, 47%). LC–MS (ESI) m/z : 390.0 (M + H)⁺; ¹H NMR (400 MHz, CDCl₃): δ 8.60–8.73 (m, 1H), 7.33–7.61 (m, 5H), 5.70–5.79 (m, 2H), 4.70–4.88 (m, 2H), 3.48–3.66 (m, 2H), 0.82–1.12 (m, 2H), –0.05–0.01 (m, 9H).

[3-(4,6-Dichloro-7-[[2-(trimethylsilyl)ethoxy]methyl]-7H-pyrrolo[2,3-d]pyrimidin-5-yl)phenyl]methanol (S5). A flask was charged with [3-(4-chloro-7-[[2-(trimethylsilyl)ethoxy]methyl]-7H-pyrrolo[2,3-d]pyrimidin-5-yl)phenyl]methanol **S4** (4.3 g, 11.0 mmol), triphenylphosphine sulfide (1.62 g, 5.51 mmol), and chloroform (50 mL). The solution was cooled to 15 °C, and NCS (3.09 g, 23.2 mmol) was added in 10 portions. The reaction was allowed to warm to 25 °C and stirred for 16 h. An aqueous solution of saturated sodium sulfite (50 mL) was added, and the mixture was stirred for 10 min and diluted with DCM (300 mL) and water (50 mL). The layers were separated, and the aqueous layer was extracted with DCM (2 × 100 mL). The combined organic layer was washed with an aqueous solution of saturated sodium bicarbonate (200 mL) and brine (200 mL) and then dried over anhydrous sodium sulfate, filtered, and concentrated in vacuo to provide the crude product as a yellow oil. The crude material was purified using column chromatography (3:1

petroleum ether/ethyl acetate) to provide the title compound as a yellow oil (500 mg, 11%). LC–MS (ESI) m/z : 424.0 (M + H)⁺; ¹H NMR (400 MHz, CDCl₃): δ 8.67 (s, 1H), 7.53–7.34 (m, 4H), 5.79 (s, 2H), 4.79 (s, 2H), 3.67 (dd, J = 7.7, 8.7 Hz, 2H), 1.00–0.92 (m, 2H), –0.03 (s, 9H).

tert-Butyl [(2S*)-4-(6-Chloro-5-[3-(hydroxymethyl)phenyl]-7-[[2-(trimethylsilyl)ethoxy]methyl]-7H-pyrrolo[2,3-d]pyrimidin-4-yl)morpholin-2-yl]methyl]carbamate (S6). A flask was charged with [3-(4,6-dichloro-7-[[2-(trimethylsilyl)ethoxy]methyl]-7H-pyrrolo[2,3-d]pyrimidin-5-yl)phenyl]methanol **S5** (250 mg, 0.589 mmol), *tert*-butyl (morpholin-2-ylmethyl)carbamate (191 mg, 0.884 mmol) and *n*-butanol (10 mL). DIPEA (0.41 mL, 2.36 mmol) was added and the reaction was heated to 105 °C for 40 h. The reaction was cooled, diluted with water (30 mL) and extracted with ethyl acetate (3 × 20 mL). The combined organic layer was washed with brine (30 mL), dried over anhydrous sodium sulfate, filtered and concentrated to provide a yellow oil. The crude material was purified using column chromatography (2:1 petroleum ether/ethyl acetate) to provide a yellow gum. The material was further purified using acidic HPLC (54–84% acetonitrile in 0.2% aqueous formic acid, flow rate = 25 mL/min, gradient time = 10 min, Agela ASB DuraShell C18, 150 mm × 25 mm × 5 μm column). Fractions were basified using an aqueous solution of saturated sodium bicarbonate, separated and the aqueous phase was extracted with ethyl acetate (2 × 50 mL). The combined organic layer was washed with brine (50 mL), dried over anhydrous sodium sulfate, filtered, and concentrated to provide a white gum. The resulting racemic material was purified using SFC (40, 0.1% NH₃, H₂O ethanol in carbon dioxide, flow rate = 60 mL/min, back pressure = 100 ba, Phenomenex Lux cellulose-2, 250 mm × 30 mm × 10 μm column, peak 2) to provide the title compound as a white solid (77 mg, 39%). LC–MS (ESI) m/z : 604.1 (M + H)⁺; ¹H NMR (400 MHz, CDCl₃): δ 8.48 (s, 1H), 7.58 (br s, 1H), 7.49–7.35 (m, 2H), 7.25–7.17 (m, 1H), 5.81–5.65 (m, 2H), 4.77 (br s, 3H), 3.92–3.78 (m, 2H), 3.71–3.63 (m, 2H), 3.57–3.46 (m, 1H), 3.27 (br d, J = 13.1 Hz, 1H), 3.00–2.89 (m, 1H), 2.81–2.70 (m, 2H), 2.99–2.55 (m, 1H), 2.53 (br s, 1H), 2.32 (br t, J = 11.4 Hz, 1H), 1.45 (s, 9H), 0.96 (dd, J = 7.8, 8.8 Hz, 2H), 0.03–0.16 (m, 9H).

3-{4-[(2S*)-2-(Aminomethyl)morpholin-4-yl]-6-chloro-7H-pyrrolo[2,3-d]pyrimidin-5-yl}phenyl]methanol (4). A flask was charged with *tert*-butyl [(2S*)-4-(6-chloro-5-[3-(hydroxymethyl)phenyl]-7-[[2-(trimethylsilyl)ethoxy]methyl]-7H-pyrrolo[2,3-d]pyrimidin-4-yl)morpholin-2-yl]methyl]carbamate **S6** (77 mg, 0.229 mmol) and DCM (3 mL). Trifluoroacetic acid (9 mL) was added, and the reaction was allowed to stir at 30 °C for 3 h. The reaction mixture was concentrated in vacuo, and the resulting material was dissolved in methanol (5 mL) and aqueous ammonia (5 mL). The reaction was stirred at 30 °C for 16 h and then concentrated in vacuo. The resulting material was purified using acidic HPLC (0–30% acetonitrile in 0.2% aqueous formic acid, gradient time = 11 min, flow rate = 30 mL/min, Agela DuraShell C18, 150 mm × 25 mm × 5 μm column) to provide the title compound as a white solid (21.3 mg, 42%). LC–MS (ESI) m/z : 374.3 (M + H)⁺; ¹H NMR (400 MHz, methanol-*d*₄): δ 8.52 (br s, 1H), 8.31 (s, 1H), 7.52–7.31 (m, 4H), 4.69 (s, 2H), 3.71–3.59 (m, 2H), 3.54 (br d, J = 13.1 Hz, 1H), 3.43–3.29 (m, 3H), 2.83–2.74 (m, 1H), 2.72–2.61 (m, 2H), 2.54 (dd, J = 10.3, 12.8 Hz, 1H).

3-{4-[(3R,5S)-3-Amino-5-methylpiperidin-1-yl]-6-chloro-7H-pyrrolo[2,3-d]pyrimidin-5-yl}benzotrile (11). A microwave vial was charged with 3-(4,6-dichloro-7-[[2-(trimethylsilyl)ethoxy]methyl]-7H-pyrrolo[2,3-d]pyrimidin-5-yl)benzotrile **28** (737 mg, 1.76 mmol), *tert*-butyl [(3R,5S)-5-methylpiperidin-3-yl]carbamate (446 mg, 2.02 mmol), and acetonitrile (3.5 mL). DIPEA (0.61 mL, 3.15 mmol) was added, and the reaction was heated to 140 °C in a microwave for 3 h. The reaction was concentrated to provide a yellow foam. The crude material was dissolved in DCM (4.4 mL), and trifluoroacetic acid (4.4 mL) was added. The reaction was allowed to stir for 6 h, at which point trifluoroacetic acid (1 mL) was added. After 2 h of stirring, the reaction was concentrated in vacuo, and the resulting material was dissolved in methanol (8.7 mL). Potassium

carbonate (1.37 g, 8.79 mmol) was added. The reaction was stirred for 16 h and then concentrated. The crude material was purified using SFC (25% methanol in carbon dioxide with pressure at 120 bar, flow rate = 90 mL/min, coupled two ZymorSpher HAP, 150 mm × 21.2 mm × 5 μm column at 40 °C) to provide the title compound (270 mg, 42%). LC–MS (APCI) m/z : 367.0 (M + H)⁺; ¹H NMR (400 MHz, methanol-*d*₄): δ 8.36 (s, 1 H) 7.74–7.86 (m, 3 H) 7.64–7.72 (m, 1 H) 4.20 (d, J = 12.0 Hz, 1H), 3.44 (d, J = 11.7 Hz, 1H), 3.00 (t, J = 11.1 Hz, 1H), 2.52 (t, J = 11.6 Hz, 1H), 1.99–2.11 (m, 1H), 1.94 (d, J = 12.0 Hz, 1H), 1.10–1.22 (m, 1H), 0.93 (q, J = 11.7 Hz, 1H), 0.60 (d, J = 6.4 Hz, 3 H).

3-[6-Chloro-4-(9-methyl-1-oxa-4,9-diazaspiro[5.5]undec-4-yl)-7-[[2-(trimethylsilyl)ethoxy]methyl]-7H-pyrrolo[2,3-d]pyrimidin-5-yl]benzotrile (S7). A flask was charged with 3-(4,6-dichloro-7-[[2-(trimethylsilyl)ethoxy]methyl]-7H-pyrrolo[2,3-d]pyrimidin-5-yl)benzotrile **28** (220 mg, 0.525 mmol), 9-methyl-1-oxa-4,9-diazaspiro[5.5]undecane (191 mg, 0.787 mmol), and *n*-butanol (10 mL). DIPEA (0.55 mL, 3.15 mmol) was added, and the reaction was heated to 105 °C for 16 h. The mixture was concentrated to yield an oil, which was purified using column chromatography (10:1 DCM/methanol) to provide the title compound as a yellow oil (280 mg, 97%). LC–MS (ESI) m/z : 553.2 (M + H)⁺; ¹H NMR (400 MHz, CDCl₃): δ 8.51 (s, 1H), 7.82 (d, J = 7.8 Hz, 1H), 7.74 (s, 1H), 7.66–7.70 (m, 1H), 7.59–7.64 (m, 1H), 5.75 (s, 2H), 3.66–3.70 (m, 2H), 3.27 (br s, 2H), 3.15–3.20 (m, 2H), 2.98 (br s, 2H), 2.73 (s, 3H), 2.15–2.25 (m, 2H), 2.04–2.12 (m, 2H), 1.50–1.53 (m, 2H), 1.46 (br s, 2H), 0.93–1.01 (m, 2H), 0.03 (s, 9H).

3-[6-Chloro-4-(9-methyl-1-oxa-4,9-diazaspiro[5.5]undec-4-yl)-7H-pyrrolo[2,3-d]pyrimidin-5-yl]benzotrile (2). A flask was charged with 3-[6-chloro-4-(9-methyl-1-oxa-4,9-diazaspiro[5.5]undec-4-yl)-7-[[2-(trimethylsilyl)ethoxy]methyl]-7H-pyrrolo[2,3-d]pyrimidin-5-yl]benzotrile **S7** (280 mg, 0.506 mmol) and DCM (3 mL). Trifluoroacetic acid (9 mL) was added at 30 °C, and the reaction was allowed to stir for 3 h. The mixture was concentrated in vacuo to provide a yellow oil. The crude material was purified using HPLC (7–27% acetonitrile in 0.2% aqueous formic acid, gradient time = 10 min, flow rate = 30 mL/min, Agela DuraShell C18, 150 mm × 25 mm × 5 μm column) to provide the title compound as a white solid (57.1 mg, 27%). LC–MS (ESI) m/z : 432.0 (M + H)⁺; ¹H NMR (400 MHz, methanol-*d*₄): δ 8.51 (br s, 1H), 8.40 (s, 1H), 7.84–7.91 (m, 2H), 7.78–7.82 (m, 1H), 7.70–7.75 (m, 1H), 3.27–3.33 (m, 4H), 3.10–3.20 (m, 4H), 2.95–3.00 (m, 2H), 2.85 (s, 3H), 2.21 (br d, J = 14.3 Hz, 2H), 1.74–1.85 (m, 2H).

3-(4,6-Dichloro-7-[[2-(trimethylsilyl)ethoxy]methyl]-7H-pyrrolo[2,3-d]pyrimidin-5-yl)-2-methylbenzotrile (S8). A flask was charged with 4,6-dichloro-5-iodo-7-[[2-(trimethylsilyl)ethoxy]methyl]-7H-pyrrolo[2,3-d]pyrimidine **27** (500 mg, 1.13 mmol), (3-cyano-2-methylphenyl)boronic acid (199 mg, 1.24 mmol), dichloro *bis*[di-*tert*-butyl(4-dimethylaminophenyl)phosphine]palladium(II) (79.7 mg, 0.113 mmol), tripotassium phosphate (717 mg, 3.38 mmol), dioxane (15 mL), and water (2 mL). The mixture was degassed and purged with nitrogen gas three times and heated to 70 °C for 16 h. The reaction was cooled to room temperature and diluted with water (5 mL). The mixture was extracted with ethyl acetate (2 × 10 mL). The combined organic layer was dried over anhydrous sodium sulfate, filtered, and concentrated. The resulting crude material was purified using column chromatography (0–10% ethyl acetate in petroleum ether) to provide the title compound as a yellow gum (150 mg, 31%). LC–MS (ESI) m/z : 432.9 (M + H)⁺; ¹H NMR (400 MHz, DMSO-*d*₆): δ 8.79 (s, 1H), 7.94 (br d, J = 7.5 Hz, 1H), 7.66 (br d, J = 7.5 Hz, 1H), 7.54 (t, J = 7.7 Hz, 1H), 5.77 (s, 2H), 3.64 (br t, J = 7.8 Hz, 2H), 2.29 (s, 3H), 0.86 (br t, J = 7.8 Hz, 2H), –0.09 (s, 9H).

tert-Butyl [(3R,5S)-1-[6-Chloro-5-(3-cyano-2-methylphenyl)-7-[[2-(trimethylsilyl)ethoxy]methyl]-7H-pyrrolo[2,3-d]pyrimidin-4-yl]-5-methylpiperidin-3-yl]carbamate (S9). A flask was charged with 3-(4,6-dichloro-7-[[2-(trimethylsilyl)ethoxy]methyl]-7H-pyrrolo[2,3-d]pyrimidin-5-yl)-2-methylbenzotrile **S8** (130 mg, 0.30 mmol), *tert*-butyl [(3R,5S)-5-methylpiperidin-3-yl]carbamate (70.7 mg, 0.33 mmol), and acetonitrile (5 mL).

DIPEA (0.16 mL, 0.90 mmol) was added, and the reaction was heated to 60 °C for 16 h. The mixture was cooled to room temperature, combined with another reaction run on 20 mg scale, and was concentrated in vacuo. The resulting material was purified using column chromatography [0–10% ethyl acetate in petroleum ether to provide the title compound as a yellow gum (150 mg, average yield 71%)]. LC–MS (ESI) m/z : 611.1 (M + H)⁺; ¹H NMR (400 MHz, DMSO-*d*₆): δ 8.43 (d, *J* = 6.3 Hz, 1H), 7.89 (br d, *J* = 8.0 Hz, 1H), 7.38–7.70 (m, 2H), 6.79 (br d, *J* = 7.0 Hz, 1H), 5.58–5.73 (m, 2H), 3.67–3.91 (m, 1H), 3.63 (br t, *J* = 7.8 Hz, 2H), 3.49 (br s, 1H), 3.03 (br s, 1H), 2.23–2.46 (m, 3H), 2.00–2.21 (m, 2H), 1.57–1.76 (m, 1H), 1.39 (d, *J* = 3.8 Hz, 9H), 0.75–0.99 (m, 4H), 0.46–0.59 (m, 3H), –0.10 (d, *J* = 1.8 Hz, 9H).

3-{4-[(3*R*,5*S*)-3-Amino-5-methylpiperidin-1-yl]-6-chloro-7*H*-pyrrolo[2,3-*d*]pyrimidin-5-yl}-2-methylbenzotrile (16). A vial was charged with *tert*-butyl [(3*R*,5*S*)-1-[6-chloro-5-(3-cyano-2-methylphenyl)-7-[[2-(trimethylsilyl)ethoxy]methyl]-7*H*-pyrrolo[2,3-*d*]pyrimidin-4-yl]-5-methylpiperidin-3-yl]carbamate **S9** (150 mg, 0.245 mmol) and DCM (6 mL). Trifluoroacetic acid (3 mL) was added, and the reaction was allowed to stir for 2 h. The reaction was concentrated in vacuo and the resulting residue was diluted with 1,4-dioxane (5 mL) and concentrated ammonium hydroxide (2 mL). The mixture was stirred for 20 min and concentrated in vacuo. The crude material was isolated as a mixture of atropdiastereomers and was purified using HPLC (20–60% acetonitrile in 0.05% v/v aqueous ammonium hydroxide, gradient time = 12 min, flow rate = 25 mL/min, Agela DuraShell C18, 150 mm × 25 mm × 5 μm) to provide the title compound as a white solid (65 mg, 99%). Notably, after separation and lyophilization each atropisomer equilibrated to a mixture of atropdiastereomers. LC–MS (ESI) m/z : 381.2 (M + H)⁺; ¹H NMR (400 MHz, DMSO-*d*₆): δ 8.28 (d, *J* = 1.5 Hz, 1H), 7.84 (d, *J* = 7.3 Hz, 1H), 7.66–7.43 (m, 2H), 3.88 (br d, *J* = 11.8 Hz, 1H), 3.78 (br d, *J* = 11.3 Hz, 1H), 3.33 (br t, *J* = 10.8 Hz, 1H), 2.39–2.20 (m, 3H), 2.18–2.04 (m, 1H), 1.99–1.83 (m, 1H), 1.68 (br t, *J* = 13.4 Hz, 1H), 0.80 (br s, 1H), 0.68–0.57 (m, 1H), 0.56–0.38 (m, 3H).

3-(4,6-Dichloro-7-[[2-(trimethylsilyl)ethoxy]methyl]-7*H*-pyrrolo[2,3-*d*]pyrimidin-5-yl)-2-fluorobenzotrile (S10). A flask was charged with 4,6-dichloro-5-iodo-7-[[2-(trimethylsilyl)ethoxy]methyl]-7*H*-pyrrolo[2,3-*d*]pyrimidine **27** (200 mg, 0.45 mmol), (3-cyano-2-fluorophenyl)boronic acid (89 mg, 0.54 mmol), dichloro bis[di-*tert*-butyl(4-dimethylaminophenyl)phosphine]-palladium(II) (32 mg, 0.045 mmol), tripotassium phosphate (287 mg, 1.25 mmol), dioxane (7 mL) and water (1 mL). The mixture was degassed and purged with nitrogen three times. The reaction was heated to 70 °C for 16 h at which point it was diluted with water (10 mL) and extracted with ethyl acetate (2 × 20 mL). The combined organic layer was dried over anhydrous sodium sulfate, filtered, and concentrated. The crude material was purified using column chromatography (5:1 petroleum ether/ethyl acetate) to provide the title compound as a pale-yellow gum (80 mg, 41%). LC–MS (ESI) m/z : 436.9 (M + H)⁺; ¹H NMR (400 MHz, DMSO-*d*₆): δ 8.83 (s, 1H), 8.12 (t, *J* = 6.7 Hz, 1H), 7.96 (t, *J* = 7.5 Hz, 1H), 7.61 (t, *J* = 7.8 Hz, 1H), 5.81–5.76 (m, 2H), 3.68–3.60 (m, 2H), 0.87 (t, *J* = 7.9 Hz, 2H), –0.08 (s, 9H).

***tert*-Butyl [(3*R*,5*S*)-1-[6-Chloro-5-(3-cyano-2-fluorophenyl)-7-[[2-(trimethylsilyl)ethoxy]methyl]-7*H*-pyrrolo[2,3-*d*]pyrimidin-4-yl]-5-methylpiperidin-3-yl]carbamate (S11).** A flask was charged with 3-(4,6-dichloro-7-[[2-(trimethylsilyl)ethoxy]methyl]-7*H*-pyrrolo[2,3-*d*]pyrimidin-5-yl)-2-fluorobenzotrile **S10** (80 mg, 0.18 mmol), *tert*-butyl [(3*R*,5*S*)-5-methylpiperidin-3-yl]-carbamate (47 mg, 0.22 mmol), and *n*-butanol (2 mL). DIPEA (0.1 mL, 0.549 mmol) was added, and the reaction was heated to 135 °C for 24 h. The reaction was concentrated and purified using column chromatography (2:1 petroleum ether/ethyl acetate) to provide the title compound (50 mg, 44%). LC–MS (ESI) m/z : 615.1 (M + H)⁺; ¹H NMR (400 MHz, DMSO-*d*₆): δ 8.45 (d, *J* = 3.8 Hz, 1H), 8.10–8.00 (m, 1H), 7.82 (br t, *J* = 7.0 Hz, 1H), 7.61–7.53 (m, 1H), 6.83–6.71 (m, 1H), 5.73–5.63 (m, 2H), 3.84–3.70 (m, 1H), 3.63 (br t, *J* = 7.4 Hz, 2H), 3.56 (br s, 1H), 3.08 (td, *J* = 2.0, 3.8 Hz, 1H), 2.23–2.04 (m, 2H), 1.76–1.63 (m, 1H), 1.38 (br d, *J* = 4.5 Hz, 9H), 1.22–0.99

(m, 1H), 0.93–0.77 (m, 3H), 0.67–0.54 (m, 3H), –0.09 (d, *J* = 3.0 Hz, 9H).

***tert*-Butyl [(3*R*,5*S*)-1-[6-Chloro-5-(3-cyano-2-fluorophenyl)-7-[[2-(trimethylsilyl)ethoxy]methyl]-7*H*-pyrrolo[2,3-*d*]pyrimidin-4-yl]-5-methylpiperidin-3-yl]carbamate (18).** A flask was charged with *tert*-butyl [(3*R*,5*S*)-1-[6-chloro-5-(3-cyano-2-fluorophenyl)-7-[[2-(trimethylsilyl)ethoxy]methyl]-7*H*-pyrrolo[2,3-*d*]pyrimidin-4-yl]-5-methylpiperidin-3-yl]carbamate **S11** (100 mg, 0.16 mmol), DCM (2 mL), and trifluoroacetic acid (5 mL). The reaction was allowed to stir at 20 °C for 1 h. The reaction was concentrated in vacuo, diluted with THF, and re-concentrated in vacuo. The resulting material was dissolved in methanol, and ammonium hydroxide was added dropwise until the pH was 7–8. The resulting material was purified using HPLC (26–46% acetonitrile in 0.05% v/v aqueous ammonium hydroxide, gradient time = 10 min, flow rate = 30 mL/min, Agela DuraShell C18, 150 mm × 25 mm × 5 μm) to provide the title compound as a white solid (63 mg, 48%). LC–MS (ESI) m/z : 385.0 (M + H)⁺; ¹H NMR (400 MHz, DMSO-*d*₆): δ 8.26 (s, 1H), 7.93 (br t, *J* = 6.0 Hz, 1H), 7.85–7.62 (m, 1H), 7.55–7.44 (m, 1H), 3.88 (br s, 1H), 3.35 (br d, *J* = 10.5 Hz, 1H), 2.64–2.54 (m, 1H), 2.24 (br s, 1H), 1.95 (br d, *J* = 9.0 Hz, 1H), 1.76 (br s, 1H), 0.94 (br s, 1H), 0.73 (q, *J* = 11.2 Hz, 1H), 0.53 (br d, *J* = 6.3 Hz, 3H).

***rac-tert*-Butyl [(3*aR**,7*aR**)-4-[6-Chloro-5-(3-cyanophenyl)-7-[[2-(trimethylsilyl)ethoxy]methyl]-7*H*-pyrrolo[2,3-*d*]pyrimidin-4-yl]octahydro-1*H*-pyrrolo[3,2-*b*]pyridine-1-carboxylate (S12).** A microwave vial was charged with 3-(4,6-dichloro-7-[[2-(trimethylsilyl)ethoxy]methyl]-7*H*-pyrrolo[2,3-*d*]pyrimidin-5-yl)benzotrile **28** (202 mg, 0.482 mmol), *rac-tert*-butyl [(3*aR**,7*aR**)-octahydro-1*H*-pyrrolo[3,2-*b*]pyridine-1-carboxylate (120 mg, 0.530 mmol), and acetonitrile (2.4 mL). DIPEA (0.4 mL, 2.41 mmol) was added, and the reaction was heated to 100 °C in a microwave for 2 h and 120 °C in a microwave for 8 h. The solution was concentrated in vacuo and purified using column chromatography (0–100% ethyl acetate in heptane) to provide the title compound as a pale-yellow foam (175 mg, 60%). LC–MS (APCI) m/z : 610.3 (M + H)⁺; ¹H NMR (400 MHz, CDCl₃): δ 8.54 (s, 1H), 7.78 (br s, 1H), 7.70 (d, *J* = 7.7 Hz, 1H), 7.56–7.57 (m, 1H), 7.54–7.65 (m, 1H), 5.76 (s, 2H), 4.47–4.71 (m, 1H), 3.68–3.79 (m, 2H), 3.35–3.47 (m, 2H), 3.12–3.28 (m, 1H), 2.56–2.78 (m, 1H), 1.96–2.14 (m, 2H), 1.48 (s, 9H), 1.21–1.32 (m, 5H), 0.96–1.05 (m, 2H), –0.10–0.05 (m, 9H).

3-[6-Chloro-4-[(3*aR*,7*aR*)-octahydro-4*H*-pyrrolo[3,2-*b*]pyridin-4-yl]-7*H*-pyrrolo[2,3-*d*]pyrimidin-5-yl]benzotrile (20). A vial was charged with *rac-tert*-butyl [(3*aR*,7*aR*)-4-[6-chloro-5-(3-cyanophenyl)-7-[[2-(trimethylsilyl)ethoxy]methyl]-7*H*-pyrrolo[2,3-*d*]pyrimidin-4-yl]octahydro-1*H*-pyrrolo[3,2-*b*]pyridine-1-carboxylate **S12** (175 mg, 0.287 mmol), DCM (3 mL), and trifluoroacetic acid (1 mL). The reaction was allowed to stir at room temperature for 2 h. The mixture was concentrated in vacuo and azeotroped with toluene (3×). The resulting material was dissolved in methanol (3 mL) and a 7 N solution of ammonia in methanol (3 mL). The solution was stirred at room temperature for 4 h and concentrated in vacuo. The material was azeotroped with toluene (3×). The crude material was purified, and the enantiomers were separated using SFC (40% methanol + 10 mM ammonia in carbon dioxide with pressure at 120 bar, flow rate = 4 mL/min, Chiral Technologies Chiralpak AS-3, 4.6 mm × 100 mm × 3 μm column, peak 1). This provided the title compound (44 mg, 40%). LC–MS (APCI) m/z : 379.1 (M + H)⁺; ¹H NMR (400 MHz, DMSO-*d*₆): δ 8.34 (s, 1H), 7.76–7.78 (m, 3H), 7.67–7.69 (m, 1H), 4.23–4.29 (m, 1H), 2.72–2.87 (m, 4H), 1.64–1.82 (m, 2H), 1.47–1.51 (m, 1H), 1.25–1.38 (m, 2H), 1.09–1.13 (m, 1H), 0.95–1.05 (m, 1H), 0.83–0.90 (m, 1H).

3-[4-[(3*S*,4*R*)-3-Amino-4-fluoropiperidin-1-yl]-6-chloro-7*H*-pyrrolo[2,3-*d*]pyrimidin-5-yl]benzotrile (21). A microwave vial was charged with 3-(4,6-dichloro-7-[[2-(trimethylsilyl)ethoxy]methyl]-7*H*-pyrrolo[2,3-*d*]pyrimidin-5-yl)benzotrile **28** (104 mg, 0.248 mmol), *tert*-butyl [(3*S*,4*R*)-4-fluoropiperidin-3-yl]carbamate (81 mg, 0.372 mmol), acetonitrile (1.2 mL), and DIPEA (0.3 mL, 1.91 mmol). The reaction was heated to 140 °C for 1 h and then directly purified using column chromatography (0–100% ethyl acetate in heptane). The resulting material was dissolved in DCM

(5 mL) and trifluoroacetic acid (1 mL). The mixture was stirred for 1 h, then concentrated, and subsequently dissolved in 3 N ammonia in methanol (3 mL). The reaction was concentrated in vacuo, and the resulting material was purified using SFC (15–50% methanol in carbon dioxide @100 bar, flow rate = 60 mL/min, ZymorSpher HADP, 21.1 mm × 150 mm × 5 μm column) to provide the title compound (45 mg, 49%). LC–MS (APCI) *m/z*: 370.9 (M + H)⁺; ¹H NMR (700 MHz, DMSO-*d*₆): δ 8.39 (s, 1H), 7.89–7.83 (m, 2H), 7.75 (s, 1H), 7.70 (s, 1H), 4.89–4.67 (m, 1H), 3.72–3.59 (m, 1H), 3.25 (d, *J* = 13.4 Hz, 1H), 2.94–2.87 (m, 1H), 2.82–2.78 (m, 1H), 2.74–2.67 (m, 1H), 1.68–1.59 (m, 1H), 1.39–1.24 (m, 1H).

tert-Butyl [(3*R*,6*S*)-1-(6-Chloro-5-iodo-7-[[2-(trimethylsilyl)ethoxy]methyl]-7*H*-pyrrolo[2,3-*d*]pyrimidin-4-yl)-6-methylpiperidin-3-yl]carbamate (30). A vial was charged with 4,6-dichloro-5-iodo-7-[[2-(trimethylsilyl)ethoxy]methyl]-7*H*-pyrrolo[2,3-*d*]pyrimidine 27 (100 mg, 0.225 mmol) and *tert*-butyl [(3*R*,6*S*)-6-methylpiperidin-3-yl]carbamate²⁴ (145 mg, 0.675 mmol), *n*-butanol (6 mL) and DIPEA (0.16 mL, 0.901 mmol). The reaction was heated to 125 °C for 40 h and then concentrated to provide a yellow residue. The crude material was purified using column chromatography (4:1 petroleum ether/ethyl acetate) to provide the title compound as a yellow gum (100 mg, 71%). LC–MS (ESI) *m/z*: 622.1 (M + H)⁺; ¹H NMR (400 MHz, DMSO-*d*₆): δ 8.51 (s, 1H), 7.06 (br d, *J* = 7.9 Hz, 1H), 5.80–5.69 (m, 2H), 4.57 (br s, 1H), 3.80 (br d, *J* = 9.4 Hz, 1H), 3.66 (br t, *J* = 7.7 Hz, 2H), 3.56 (br s, 1H), 3.19–3.07 (m, 1H), 2.38–2.14 (m, 1H), 1.89–1.65 (m, 3H), 1.51 (s, 9H), 1.12 (br d, *J* = 6.3 Hz, 3H), 0.93 (br t, *J* = 7.8 Hz, 2H), 0.00 (s, 9H).

tert-Butyl [(3*R*,6*S*)-1-(6-Chloro-5-(3-cyanophenyl)-7-[[2-(trimethylsilyl)ethoxy]methyl]-7*H*-pyrrolo[2,3-*d*]pyrimidin-4-yl)-6-methylpiperidin-3-yl]carbamate (31). A microwave vial was charged with *tert*-butyl [(3*R*,6*S*)-1-(6-chloro-5-iodo-7-[[2-(trimethylsilyl)ethoxy]methyl]-7*H*-pyrrolo[2,3-*d*]pyrimidin-4-yl)-6-methylpiperidin-3-yl]carbamate 30 (100 mg, 0.161 mmol), 1,4-dioxane (8 mL), water (2 mL), (3-cyanophenyl)boronic acid (47.2 mg, 0.322 mmol), potassium carbonate (66.7 mg, 0.482 mmol), and [1,1'-bis(diphenylphosphino)ferrocene]dichloropalladium(II) (11.8 mg, 0.016 mmol). The mixture was bubbled with nitrogen for 5 min and heated to 100 °C in a microwave for 2 h. The reaction was diluted with ethyl acetate (30 mL) and washed with brine (30 mL). The organic layer was dried over anhydrous sodium sulfate, filtered, and concentrated to provide a yellow residue, which was purified using column chromatography (3:1 petroleum ether/ethyl acetate) to provide the title compound as a yellow gum (84 mg, 87%). LC–MS (ESI) *m/z*: 597.3 (M + H)⁺; ¹H NMR (400 MHz, CDCl₃): δ 8.48 (s, 1H), 7.79 (br s, 1H), 7.71–7.63 (m, 2H), 7.61–7.53 (m, 1H), 5.72 (s, 2H), 4.28 (br s, 1H), 4.15–4.04 (m, 1H), 3.78–3.61 (m, 3H), 3.34 (br s, 1H), 3.42–2.85 (m, 1H), 2.45 (t, *J* = 11.9 Hz, 1H), 1.42 (s, 9H), 1.37–1.18 (m, 4H), 0.97 (dd, *J* = 7.0, 9.3 Hz, 2H), 0.91 (d, *J* = 7.0 Hz, 3H), –0.03 (s, 9H).

3-[4-[(2*S*,5*R*)-5-Amino-2-methylpiperidin-1-yl]-6-chloro-7*H*-pyrrolo[2,3-*d*]pyrimidin-5-yl]benzotriazole (19). A flask was charged with *tert*-butyl [(3*R*,6*S*)-1-(6-chloro-5-(3-cyanophenyl)-7-[[2-(trimethylsilyl)ethoxy]methyl]-7*H*-pyrrolo[2,3-*d*]pyrimidin-4-yl)-6-methylpiperidin-3-yl]carbamate 31 (84 mg, 0.140 mmol), DCM (3 mL), and trifluoroacetic acid (9 mL). The reaction was allowed to stir at 30 °C for 2 h. The reaction was concentrated in vacuo, and the resulting yellow oil was basified with 28% aqueous ammonium hydroxide to pH > 8. The solution was concentrated in vacuo and purified using HPLC (20–40% acetonitrile in 0.2% aqueous formic acid, gradient time = 10 min, flow rate = 25 mL/min, Agela ASB C18, 150 mm × 25 mm × 5 μm column) to provide the title compound as a white solid (15.5 mg, 30%). LC–MS (ESI) *m/z*: 367.1 (M + H)⁺; ¹H NMR (400 MHz, DMSO-*d*₆): δ 8.36 (s, 2H), 7.89–7.63 (m, 4H), 3.88–3.64 (m, 2H), 3.02–2.71 (m, 2H), 1.78–1.46 (m, 2H), 1.27–0.98 (m, 2H), 0.73 (d, *J* = 6.8 Hz, 3H).

tert-Butyl 6-(6-Chloro-5-iodo-7-[[2-(trimethylsilyl)ethoxy]methyl]-7*H*-pyrrolo[2,3-*d*]pyrimidin-4-yl)-2,6-diazaspiro[3.5]nonane-2-carboxylate (S13). A flask was charged with 4,6-dichloro-5-iodo-7-[[2-(trimethylsilyl)ethoxy]methyl]-7*H*-pyrrolo[2,3-*d*]pyrimidine 27 (200 mg, 0.450 mmol) and *tert*-butyl 2,6-

diazaspiro[3.5]nonane-2-carboxylate (147 mg, 0.540 mmol), *n*-butanol (5 mL), and DIPEA (0.47 mL, 2.70 mmol). The reaction was heated to 105 °C and allowed to stir for 20 h. The reaction mixture was concentrated and purified using column chromatography (0–28% ethyl acetate in petroleum ether) to provide the title compound as a yellow gum (230 mg, 81%). LC–MS (ESI) *m/z*: 634.1 (M + H)⁺; ¹H NMR (400 MHz, CDCl₃): δ 8.47 (s, 1H), 5.70 (s, 2H), 3.75–3.70 (m, 2H), 3.63 (t, *J* = 7.8 Hz, 2H), 3.62 (d, *J* = 8.0 Hz, 2H), 3.59 (s, 2H), 3.46 (br s, 2H), 1.93 (br d, *J* = 5.3 Hz, 2H), 1.86 (br d, *J* = 5.8 Hz, 2H), 1.43 (s, 9H), 0.93 (t, *J* = 7.6 Hz, 2H), –0.04 (s, 9H).

tert-Butyl 6-[6-Chloro-5-(3-cyanophenyl)-7-[[2-(trimethylsilyl)ethoxy]methyl]-7*H*-pyrrolo[2,3-*d*]pyrimidin-4-yl]-2,6-diazaspiro[3.5]nonane-2-carboxylate (S14). A flask was charged with *tert*-butyl 6-(6-chloro-5-iodo-7-[[2-(trimethylsilyl)ethoxy]methyl]-7*H*-pyrrolo[2,3-*d*]pyrimidin-4-yl)-2,6-diazaspiro[3.5]nonane-2-carboxylate S13 (130 mg, 0.205 mmol), 1,4-dioxane (6 mL), water (2 mL), (3-cyanophenyl)boronic acid (36.2 mg, 0.246 mmol), sodium carbonate (65.2 mg, 0.615 mmol), and [1,1'-bis(diphenylphosphino)ferrocene]dichloropalladium(II) (15.0 mg, 0.021 mmol). The mixture was degassed with nitrogen (3×) and heated to 85 °C for 16 h. The reaction was combined with another batch of the same reaction run on 100 mg scale, diluted with water (5 mL), and extracted with ethyl acetate (2 × 10 mL). The combined organic layer was dried over anhydrous sodium sulfate, filtered, and concentrated. The resulting material was purified using column chromatography (0–30% ethyl acetate in petroleum ether) to provide the title compound as a yellow gum (150 mg, average yield 68%). LC–MS (ESI) *m/z*: 609.2 (M + H)⁺; ¹H NMR (400 MHz, DMSO-*d*₆): δ 8.49 (s, 1H), 7.91 (br d, *J* = 7.7 Hz, 1H), 7.85 (s, 1H), 7.83–7.78 (m, 1H), 7.73 (d, *J* = 7.7 Hz, 1H), 5.68 (s, 2H), 3.62 (t, *J* = 7.9 Hz, 2H), 3.54 (br d, *J* = 7.1 Hz, 2H), 3.46 (br s, 2H), 3.31 (br s, 2H), 2.79 (br s, 2H), 1.53 (br s, 2H), 1.37 (s, 9H), 0.87 (t, *J* = 7.9 Hz, 2H), 0.75 (br d, *J* = 2.4 Hz, 2H), –0.07 (s, 9H).

3-[6-Chloro-4-(2,6-diazaspiro[3.5]non-6-yl)-7*H*-pyrrolo[2,3-*d*]pyrimidin-5-yl]benzotriazole (5). A flask was charged with *tert*-butyl 6-[6-chloro-5-(3-cyanophenyl)-7-[[2-(trimethylsilyl)ethoxy]methyl]-7*H*-pyrrolo[2,3-*d*]pyrimidin-4-yl]-2,6-diazaspiro[3.5]nonane-2-carboxylate S14 (150 mg, 0.246), DCM (10 mL), and trifluoroacetic acid (2 mL). The solution was allowed to stir at 20 °C for 3.5 h. The reaction was concentrated in vacuo, and the resulting residue was diluted with 1,4-dioxane (10 mL) and concentrated ammonium hydroxide (2 mL). The reaction was stirred for 10 min, concentrated, and purified using HPLC (22–52% acetonitrile in 0.05% v/v aqueous ammonium hydroxide, gradient time = 12 min, flow rate = 25 mL/min, Welch Materials Inc. Xtimate C18, 150 mm × 25 mm × 5 μm) to provide the title compound as a white solid (51 mg, 96%). LC–MS (ESI) *m/z*: 379.1 (M + H)⁺; ¹H NMR (400 MHz, D₂O): δ 8.48 (s, 1H), 7.87 (br d, *J* = 7.6 Hz, 1H), 7.83 (s, 1H), 7.80–7.76 (m, 1H), 7.75–7.69 (m, 1H), 3.94–3.83 (m, 4H), 3.64 (s, 2H), 3.14 (br t, *J* = 5.2 Hz, 2H), 1.78 (br t, *J* = 5.8 Hz, 2H), 0.93 (br s, 2H).

tert-Butyl [(3*S*)-1-(6-Chloro-5-iodo-7-[[2-(trimethylsilyl)ethoxy]methyl]-7*H*-pyrrolo[2,3-*d*]pyrimidin-4-yl)pyrrolidin-3-yl]carbamate (S15). A flask was charged with 4,6-dichloro-5-iodo-7-[[2-(trimethylsilyl)ethoxy]methyl]-7*H*-pyrrolo[2,3-*d*]pyrimidine 27 (200 mg, 0.450 mmol), *tert*-butyl (3*S*)-pyrrolidin-3-ylcarbamate (101 mg, 0.542 mmol), *n*-butanol (5 mL), and DIPEA (0.47 mL, 2.7 mmol). The reaction was heated to 105 °C for 20 h and then concentrated in vacuo. The crude material was purified using column chromatography (4:1 petroleum ether/ethyl acetate) to provide the title compound as a light-yellow gum (256 mg, 96%). LC–MS (ESI) *m/z*: 594.1 (M + H)⁺; ¹H NMR (400 MHz, DMSO-*d*₆): δ 8.22 (s, 1H), 7.24 (br d, *J* = 4.0 Hz, 1H), 5.61 (s, 2H), 4.06 (br d, *J* = 8.1 Hz, 2H), 3.99–3.90 (m, 1H), 3.84 (br d, *J* = 5.4 Hz, 1H), 3.70 (br d, *J* = 5.9 Hz, 1H), 3.53 (t, *J* = 7.9 Hz, 2H), 2.13–2.00 (m, 1H), 1.87 (br d, *J* = 5.0 Hz, 1H), 1.38 (s, 9H), 0.83 (t, *J* = 7.9 Hz, 2H), –0.09 (s, 9H).

tert-Butyl [(3*S*)-1-(6-Chloro-5-(3-cyanophenyl)-7-[[2-(trimethylsilyl)ethoxy]methyl]-7*H*-pyrrolo[2,3-*d*]pyrimidin-4-yl)pyrrolidin-3-yl]carbamate (S16). A flask was charged with *tert*-

butyl [(3*S*)-1-(6-chloro-5-iodo-7-[[2-(trimethylsilyl)ethoxy]methyl]-7*H*-pyrrolo[2,3-*d*]pyrimidin-4-yl)pyrrolidin-3-yl]carbamate **S15** (260 mg, 0.438 mmol), 1,4-dioxane (12 mL), water (4 mL), (3-cyanophenyl)boronic acid (82 mg, 0.560 mmol), sodium carbonate (145 mg, 1.37 mmol), and [1,1'-bis(diphenylphosphino)ferrocene]-dichloropalladium(II) (34 mg, 0.046 mmol). The resulting mixture was heated to 85 °C for 16 h. The reaction was concentrated and purified using column chromatography (4:1 petroleum ether/ethyl acetate) to provide the title compound as a light-yellow gum (220 mg, 88%). LC-MS (ESI) *m/z*: 569.3 (M + H)⁺; ¹H NMR (400 MHz, DMSO-*d*₆): δ 8.35 (s, 1H), 8.00–7.93 (m, 1H), 7.88 (s, 1H), 7.75 (d, *J* = 4.8 Hz, 2H), 7.05 (br d, *J* = 6.3 Hz, 1H), 5.70 (s, 2H), 3.78 (br d, *J* = 5.4 Hz, 1H), 3.67 (t, *J* = 7.9 Hz, 2H), 3.38–3.35 (m, 1H), 3.23 (br d, *J* = 5.0 Hz, 2H), 2.85 (br dd, *J* = 5.0, 10.6 Hz, 1H), 1.85 (br s, 1H), 1.68 (br d, *J* = 6.0 Hz, 1H), 1.41 (s, 9H), 0.93 (t, *J* = 7.9 Hz, 2H), 0.00 (s, 9H).

3-{4-[(3*S*)-3-Aminopyrrolidin-1-yl]-6-chloro-7*H*-pyrrolo[2,3-*d*]pyrimidin-5-yl}benzotrile (7). A flask was charged with *tert*-butyl {[3*S*)-1-[6-chloro-5-(3-cyanophenyl)-7-[[2-(trimethylsilyl)ethoxy]methyl]-7*H*-pyrrolo[2,3-*d*]pyrimidin-4-yl]pyrrolidin-3-yl}carbamate **S16** (220 mg, 0.387 mol), DCM (10 mL), and trifluoroacetic acid (2 mL), and the reaction was allowed to stir at 20 °C for 5 h. The mixture was concentrated in vacuo, and the resulting residue was diluted with 1,4-dioxane (10 mL) and concentrated ammonium hydroxide (2 mL). The reaction was allowed to stir for 20 min and was concentrated in vacuo and then purified using HPLC (23–53% acetonitrile in 0.05% v/v aqueous ammonium hydroxide, gradient time = 10 min, flow rate = 25 mL/min, Agela DuraShell C18, 150 mm × 25 mm × 5 μm) to provide the title compound as a white solid (37 mg, 28%). LC-MS (ESI) *m/z*: 339.1 (M + H)⁺; ¹H NMR (400 MHz, DMSO-*d*₆): δ 8.20–8.15 (m, 1H), 7.86–7.83 (m, 1H), 7.83–7.79 (m, 1H), 7.70–7.61 (m, 2H), 3.29–3.17 (m, 2H), 3.12–3.03 (m, 2H), 2.74 (dd, *J* = 4.4, 10.9 Hz, 1H), 1.76–1.66 (m, 1H), 1.45–1.36 (m, 1H).

***rac-tert*-Butyl [1-(6-Chloro-5-iodo-7-[[2-(trimethylsilyl)ethoxy]methyl]-7*H*-pyrrolo[2,3-*d*]pyrimidin-4-yl)azepan-3-yl]carbamate (S17).** A flask was charged with 4,6-dichloro-5-iodo-7-[[2-(trimethylsilyl)ethoxy]methyl]-7*H*-pyrrolo[2,3-*d*]pyrimidine **27** (200 mg, 0.450 mmol), *tert*-butyl azepan-3-ylcarbamate (174 mg, 0.810 mmol), *n*-butanol (2 mL), and DIPEA (0.47 mL, 2.70 mmol). The reaction was heated to 100 °C for 16 h and then concentrated to provide a yellow gum. The crude material was purified using column chromatography (5:1 petroleum ether/ethyl acetate) to provide the title compound as a yellow gum (230 mg, 82%). LC-MS (ESI) *m/z*: 622.0 (M + H)⁺; ¹H NMR (400 MHz, CDCl₃): δ 8.30–8.43 (m, 1H), 6.35 (br s, 1H), 5.60–5.77 (m, 2H), 4.42 (br d, *J* = 13.3 Hz, 1H), 3.78–4.10 (m, 3H), 3.62–3.68 (m, 2H), 3.58 (br d, *J* = 10.5 Hz, 1H), 1.96 (br dd, *J* = 5.1, 13.8 Hz, 1H), 1.65–1.86 (m, 3H), 1.44–1.53 (m, 11H), 0.88–1.00 (m, 2H), –0.10–0.02 (m, 9H).

3-{4-[(3*R)-3-Aminoazepan-1-yl]-6-chloro-7*H*-pyrrolo[2,3-*d*]pyrimidin-5-yl}benzotrile (6).** A microwave vial was charged with *rac-tert*-butyl [1-(6-chloro-5-iodo-7-[[2-(trimethylsilyl)ethoxy]methyl]-7*H*-pyrrolo[2,3-*d*]pyrimidin-4-yl)azepan-3-yl]carbamate **S17** (230 mg, 0.370 mmol), 1,4-dioxane (6 mL), water (1.5 mL), (3-cyanophenyl)boronic acid (109 mg, 0.740 mmol), potassium carbonate (102 mg, 0.740 mmol), and [1,1'-bis(diphenylphosphino)ferrocene]dichloropalladium(II) (27.1 mg, 0.037 mmol). The reaction was degassed and purged with nitrogen gas three times and heated to 100 °C for 80 min. The mixture was concentrated to provide a black gum. The crude material was purified using column chromatography (5:1 petroleum ether/ethyl acetate) to provide a yellow gum (200 mg). This material was combined with 90 mg from another reaction, and the enantiomers were separated using SFC (20, 0.1% ammonia in methanol in carbon dioxide, flow rate = 60 mL/min, Chiral Technologies OJ 250 mm × 30 mm × 5 μm column, peak 2) to provide a yellow gum (100 mg), which was taken on to the next step directly. LC-MS (ESI) *m/z*: 597.1 (M + H)⁺. A flask was charged with the isolated gum (100 mg) and DCM (3 mL). The solution was cooled to 0 °C, and trifluoroacetic acid was added (2.5 mL). The reaction was allowed to warm to 10 °C and stirred for 16 h.

The mixture was concentrated in vacuo, and the resulting brown residue was diluted with dioxane (2 mL) and an aqueous solution of 28% aqueous ammonium hydroxide (1 mL). The reaction was allowed to stir at 10 °C for 10 min and was concentrated in vacuo. The crude material was purified using preparative HPLC (10–40% acetonitrile in 0.2% aqueous formic acid, gradient time = 11 min, flow rate = 25 mL/min, Phenomenex Synergi C18, 150 mm × 30 mm × 4 μm column) to provide the title compound as a yellow solid (44.5 mg, 23% over two steps). LC-MS (ESI) *m/z*: 367.0 (M + H)⁺; ¹H NMR (400 MHz, DMSO-*d*₆): δ 8.32 (s, 1H), 7.84–7.76 (m, 2H), 7.74–7.62 (m, 2H), 3.83–3.75 (m, 1H), 3.73–3.64 (m, 1H), 3.48 (br d, *J* = 4.2 Hz, 1H), 3.09–2.98 (m, 1H), 2.60 (br t, *J* = 10.6 Hz, 1H), 1.95–1.84 (m, 1H), 1.53 (br s, 1H), 1.29–1.07 (m, 3H), 0.97 (br d, *J* = 8.4 Hz, 1H).

Di-*tert*-butyl [5-(Trifluoromethyl)pyridin-3-yl]imidodicarbonate (33). A flask was charged with 5-(trifluoromethyl)pyridin-3-amine (3.0 g, 18.5 mmol) and DMF (100 mL) and was cooled to 0 °C under a nitrogen atmosphere. 60% sodium hydride in mineral oil (1.78 g, 74 mmol) was added, and the reaction was allowed to stir for 30 min at 0 °C. Boc anhydride (14.1 g, 64.8 mmol) was added, and the reaction was heated to 60 °C for 4 h. The mixture was diluted with ice water (200 mL) and extracted with ethyl acetate (2 × 200 mL). The combined organic layer was washed with brine, dried over anhydrous sodium sulfate, filtered, and concentrated. The crude material was purified using column chromatography (10:1 petroleum ether/ethyl acetate) to provide the title compound as a yellow solid (2.76 g, 41%). LC-MS (ESI) *m/z*: 363.0 (M + H)⁺; ¹H NMR (400 MHz, DMSO-*d*₆): δ 8.94 (d, *J* = 1.0 Hz, 1H), 8.83 (d, *J* = 2.3 Hz, 1H), 8.36 (s, 1H), 1.38 (s, 18H).

***tert*-Butyl [(3*R**,5*S**)-5-(Trifluoromethyl)piperidin-3-yl]carbamate (34).** A steel hydrogenation bomb was charged with di-*tert*-butyl [5-(trifluoromethyl)pyridin-3-yl]imidodicarbonate **33** (2.76 g, 0.762 mmol), acetic acid (70 mL), 5% rhodium on activated carbon (0.5 g), and platinum(IV) oxide (0.5 g). The mixture was sealed and stirred at 70 °C under 200 psi of hydrogen gas for 48 h. The mixture was filtered through a pad of Celite and concentrated to provide a brown oil. The crude material was purified using column chromatography (2:1 petroleum ether/ethyl acetate) to provide a white solid (1.25 g). This material was transferred to a steel hydrogenation bomb and dissolved in acetic acid (30 mL). Platinum(IV) oxide (0.25 g) and 5% rhodium on activated carbon (0.25 g) was added, and the mixture was stirred at 70 °C under 200 psi of hydrogen gas for 48 h. The mixture was filtered and concentrated in vacuo. The crude material was purified using column chromatography (10:1 DCM/methanol) to provide the title compound as a white solid (450 mg, 35%). LC-MS (ESI) *m/z*: 269.1 (M + H)⁺; ¹H NMR (400 MHz, CDCl₃): δ 4.40 (br s, 1H), 3.55 (br s, 1H), 3.33–3.19 (m, 2H), 2.52 (t, *J* = 11.7 Hz, 1H), 2.39–2.21 (m, 3H), 1.46 (s, 9H), 1.25 (q, *J* = 12.8 Hz, 1H).

***rac-tert*-Butyl [(3*R**,5*S**)-1-(6-Chloro-5-iodo-7-[[2-(trimethylsilyl)ethoxy]methyl]-7*H*-pyrrolo[2,3-*d*]pyrimidin-4-yl)-5-(trifluoromethyl)piperidin-3-yl]carbamate (S18).** A flask was charged with 4,6-dichloro-5-iodo-7-[[2-(trimethylsilyl)ethoxy]methyl]-7*H*-pyrrolo[2,3-*d*]pyrimidine **27** (500 mg, 1.13 mmol), *tert*-butyl [(3*R**,5*S**)-5-(trifluoromethyl)piperidin-3-yl]carbamate **34** (332 mg, 1.24 mmol), *n*-butanol (6 mL), and DIPEA (1.2 mL, 6.75 mmol). The reaction was heated to 105 °C for 36 h and then concentrated to provide a yellow gum. The crude material was purified using column chromatography (5:1 petroleum ether/ethyl acetate) to provide the title compound as a yellow solid (460 mg, 61%). LC-MS (ESI) *m/z*: 676.1 (M + H)⁺; ¹H NMR (400 MHz, CDCl₃): δ 8.48 (s, 1H), 5.70 (s, 2H), 4.46 (br s, 1H), 4.32–4.13 (m, 2H), 4.02 (s, 1H), 3.66–3.57 (m, 2H), 3.03–2.80 (m, 2H), 2.71 (br t, *J* = 11.9 Hz, 1H), 2.43 (br s, 1H), 1.47–1.40 (m, 9H), 0.98–0.90 (m, 2H), –0.02–0.06 (m, 9H).

3-{4-[(3*R,5*S**)-3-Amino-5-(trifluoromethyl)piperidin-1-yl]-6-chloro-7*H*-pyrrolo[2,3-*d*]pyrimidin-5-yl}benzotrile (12).** A microwave vial was charged with *tert*-butyl [(3*R**,5*S**)-1-(6-chloro-5-iodo-7-[[2-(trimethylsilyl)ethoxy]methyl]-7*H*-pyrrolo[2,3-*d*]-

pyrimidin-4-yl)-5-(trifluoromethyl)piperidin-3-yl]carbamate **S18** (180 mg, 0.266 mmol), 1,4-dioxane (5 mL), water (1 mL), (3-cyanophenyl)boronic acid (78.3 mg, 0.533 mmol), potassium carbonate (73.6 mg, 0.533 mmol), and [1,1'-bis(diphenylphosphino)ferrocene]dichloropalladium(II) (19.5 mg, 0.027 mmol). The mixture was degassed and purged with nitrogen (3×) and the resulting mixture was heated to 100 °C in a microwave for 80 min. The reaction was concentrated to provide a black gum, which was purified using column chromatography (4:1 petroleum ether/ethyl acetate) to provide a yellow solid (130 mg). The enantiomers were separated using SFC (15, 0.1% ammonium hydroxide in methanol in carbon dioxide, flow rate = 60 mL/min, Chiral Technologies AD 250 mm × 30 mm × 5 μm column, peak 1) to provide a yellow solid (88 mg). LC-MS (ESI) *m/z*: 651.1 (M + H)⁺. A flask was charged with the isolated solid (88 mg) and DCM (3 mL), and the solution was cooled to 0 °C. Trifluoroacetic acid (2.5 mL) was added, and the reaction was warmed to 25 °C and allowed to stir for 3 h. The solution was concentrated in vacuo, and the resulting brown residue was dissolved in 1,4-dioxane (2 mL) and an aqueous solution of 28% aqueous ammonium hydroxide (1 mL). The reaction was allowed to stir at 25 °C for 5 min and was concentrated to provide a yellow solid. The crude material was purified using preparative HPLC (15–45% acetonitrile in 0.2% aqueous formic acid, gradient time = 11 min, flow rate = 25 mL/min, Phenomenex Synergi C18, 150 mm × 30 mm × 4 μm column) to provide the title compound as a yellow solid (33 mg, 18% over 2 steps). LC-MS (ESI) *m/z*: 421.0 (M + H)⁺; ¹H NMR (400 MHz, D₂O): δ 8.36 (s, 1H), 8.27 (s, 1H), 7.67 (br d, *J* = 7.0 Hz, 1H), 7.59–7.46 (m, 3H), 3.95 (br d, *J* = 9.9 Hz, 1H), 3.36 (br d, *J* = 10.9 Hz, 1H), 3.15–3.02 (m, 1H), 2.64 (t, *J* = 11.7 Hz, 1H), 2.35 (t, *J* = 12.3 Hz, 1H), 2.17 (br d, *J* = 12.4 Hz, 1H), 1.73 (br d, *J* = 8.3 Hz, 1H), 1.37 (q, *J* = 12.4 Hz, 1H).

tert-Butyl [(3R,5S)-1-(6-Chloro-5-iodo-7-[[2-(trimethylsilyl)ethoxy]methyl]-7H-pyrrolo[2,3-d]pyrimidin-4-yl)-5-methylpiperidin-3-yl]carbamate (S19). A flask was charged with 4,6-dichloro-5-iodo-7-[[2-(trimethylsilyl)ethoxy]methyl]-7H-pyrrolo[2,3-d]pyrimidin 27 (100 mg, 0.225 mmol), *tert*-butyl [(3R,5S)-5-methylpiperidin-3-yl]carbamate (48 mg, 0.225 mmol), *n*-butanol (2 mL), and DIPEA (0.12 mL, 0.67 mmol). The reaction was heated to 105 °C for 20 h. The reaction was concentrated and purified using column chromatography (5:1 petroleum ether/ethyl acetate) to provide the title compound as a yellow gum (120 mg, 86%). LC-MS (ESI) *m/z*: 621.8 (M + H)⁺; ¹H NMR (400 MHz, DMSO-*d*₆): δ 8.40 (s, 1H), 6.99 (br d, *J* = 8.0 Hz, 1H), 5.70–5.55 (m, 2H), 4.17–3.86 (m, 2H), 3.54 (br t, *J* = 7.9 Hz, 3H), 2.62–2.55 (m, 1H), 2.44–2.38 (m, 1H), 2.08–1.88 (m, 2H), 1.39 (s, 9H), 1.09 (q, *J* = 12.0 Hz, 1H), 0.90 (d, *J* = 6.5 Hz, 3H), 0.82 (br t, *J* = 7.8 Hz, 2H), –0.11 (s, 9H).

tert-Butyl [(3R,5S)-1-(6-Chloro-5-phenyl-7-[[2-(trimethylsilyl)ethoxy]methyl]-7H-pyrrolo[2,3-d]pyrimidin-4-yl)-5-methylpiperidin-3-yl]carbamate (S20). A flask was charged with *tert*-butyl [(3R,5S)-1-(6-chloro-5-iodo-7-[[2-(trimethylsilyl)ethoxy]methyl]-7H-pyrrolo[2,3-d]pyrimidin-4-yl)-5-methylpiperidin-3-yl]carbamate **S19** (120 mg, 0.19 mmol), 1,4-dioxane (6 mL), water (2 mL), phenylboronic acid (28.2 mg, 0.23 mmol), sodium carbonate (61.3 mg, 0.58 mmol), and [1,1'-bis(diphenylphosphino)ferrocene]dichloropalladium(II) (14 mg, 0.019 mmol). The mixture was purged with nitrogen (3×) and heated to 85 °C for 16 h. The reaction was diluted with water (10 mL) and extracted with ethyl acetate (20 mL). The organic layer was dried over sodium sulfate, filtered, and concentrated in vacuo. The resulting residue was purified using column chromatography (3:1 petroleum ether/ethyl acetate) to provide the title compound as a yellow gum (80 mg, 72%). LC-MS (ESI) *m/z*: 572.3 (M + H)⁺; ¹H NMR (400 MHz, DMSO-*d*₆): δ 8.40 (s, 1H), 7.54–7.45 (m, 2H), 7.45–7.32 (m, 3H), 6.77 (br d, *J* = 8.3 Hz, 1H), 5.71–5.60 (m, 2H), 4.04–3.92 (m, 1H), 3.62 (br t, *J* = 7.8 Hz, 2H), 3.56 (br d, *J* = 12.5 Hz, 1H), 3.24–3.09 (m, 1H), 2.12 (br t, *J* = 11.8 Hz, 1H), 1.95 (br t, *J* = 11.8 Hz, 1H), 1.64 (br d, *J* = 11.8 Hz, 1H), 1.42–1.29 (m, 9H), 1.16–1.00 (m, 1H), 0.85 (t, *J* = 7.8 Hz, 2H), 0.82–0.73 (m, 1H), 0.45 (br d, *J* = 6.5 Hz, 3H), –0.08 (s, 9H).

(3R,5S)-1-(6-Chloro-5-phenyl-7H-pyrrolo[2,3-d]pyrimidin-4-yl)-5-methylpiperidin-3-amine (13). A flask was charged with *tert*-

butyl [(3R,5S)-1-(6-chloro-5-phenyl-7-[[2-(trimethylsilyl)ethoxy]methyl]-7H-pyrrolo[2,3-d]pyrimidin-4-yl)-5-methylpiperidin-3-yl]carbamate **S20** (80 mg, 0.14 mmol), DCM (5 mL), and trifluoroacetic acid (2 mL). The resulting solution was allowed to stir at 25 °C for 2 h. The reaction was concentrated in vacuo, and the resulting residue was dissolved in 1,4-dioxane (5 mL). The pH was adjusted to 10–11 by addition of concentrated ammonium hydroxide. The solution was allowed to stir at 25 °C for 20 min and then concentrated in vacuo. The crude material was purified using HPLC (27–47% acetonitrile in 0.05% v/v aqueous ammonium hydroxide, gradient time = 10 min, flow rate = 30 mL/min, Agela DuraShell C18, 150 mm × 25 mm × 5 μm column) to provide the title compound as a white solid (40 mg, 84%). LC-MS (ESI) *m/z*: 342.1 (M + H)⁺; ¹H NMR (400 MHz, DMSO-*d*₆): δ 8.34–8.21 (m, 1H), 7.50–7.43 (m, 2H), 7.41–7.32 (m, 3H), 3.92–3.85 (m, 1H), 2.70–2.56 (m, 1H), 2.48–2.37 (m, 1H), 2.07 (dd, *J* = 10.8, 12.3 Hz, 1H), 1.90 (t, *J* = 11.9 Hz, 1H), 1.67 (br d, *J* = 12.5 Hz, 1H), 1.21–1.08 (m, 1H), 0.60 (q, *J* = 11.8 Hz, 1H), 0.48 (d, *J* = 6.8 Hz, 3H).

tert-Butyl [(3R,5S)-1-(6-Chloro-5-(1-methyl-1H-pyrazol-4-yl)-7-[[2-(trimethylsilyl)ethoxy]methyl]-7H-pyrrolo[2,3-d]pyrimidin-4-yl)-5-methylpiperidin-3-yl]carbamate (S21). A flask was charged with *tert*-butyl [(3R,5S)-1-(6-chloro-5-iodo-7-[[2-(trimethylsilyl)ethoxy]methyl]-7H-pyrrolo[2,3-d]pyrimidin-4-yl)-5-methylpiperidin-3-yl]carbamate **S19** (120 mg, 0.193 mmol), (1-methyl-1H-pyrazol-4-yl)boronic acid (49 mg, 0.24 mmol), 1,4-dioxane (9 mL), water (3 mL), sodium carbonate (62 mg, 0.58 mmol), and [1,1'-bis(diphenylphosphino)ferrocene]dichloropalladium(II) (15 mg, 0.021 mmol). The resulting mixture was degassed and purged with nitrogen (3×) and then heated to 85 °C for 16 h. The reaction was concentrated, and the resulting material was purified using column chromatography (4:1 petroleum ether/ethyl acetate) to provide the title compound as a light-yellow gum (220 mg, 88%). LC-MS (ESI) *m/z*: 576.3 (M + H)⁺; ¹H NMR (400 MHz, DMSO-*d*₆): δ 8.37 (s, 1H), 7.86 (s, 1H), 7.52 (s, 1H), 6.83 (br d, *J* = 7.5 Hz, 1H), 5.63 (s, 2H), 4.00 (br d, *J* = 10.8 Hz, 1H), 3.92 (s, 3H), 3.63 (br d, *J* = 13.1 Hz, 1H), 3.58 (br t, *J* = 7.9 Hz, 2H), 2.46–2.37 (m, 1H), 2.27 (t, *J* = 12.0 Hz, 1H), 2.07 (t, *J* = 12.0 Hz, 1H), 1.79–1.72 (m, 1H), 1.38 (s, 9H), 1.24 (br s, 1H), 0.85 (br t, *J* = 7.9 Hz, 3H), 0.60 (br d, *J* = 6.3 Hz, 3H), –0.09 (s, 9H).

(3R,5S)-1-[6-Chloro-5-(1-methyl-1H-pyrazol-4-yl)-7H-pyrrolo[2,3-d]pyrimidin-4-yl]-5-methylpiperidin-3-amine (14). A flask was charged with *tert*-butyl [(3R,5S)-1-(6-chloro-5-(1-methyl-1H-pyrazol-4-yl)-7-[[2-(trimethylsilyl)ethoxy]methyl]-7H-pyrrolo[2,3-d]pyrimidin-4-yl)-5-methylpiperidin-3-yl]carbamate **S21** (70 mg, 0.12 mmol), DCM (4 mL), and trifluoroacetic acid (5 mL). The reaction was allowed to stir at 25 °C for 2 h. The reaction was concentrated in vacuo to provide a residue, which was diluted with 1,4-dioxane (10 mL) and concentrated ammonium hydroxide (1 mL). The reaction was allowed to stir for 20 min and then was concentrated in vacuo. The resulting material was purified using HPLC (9–49% acetonitrile in 0.2% aqueous formic acid, gradient time = 12 min, flow rate = 25 mL/min, Agela DuraShell C18, 150 mm × 25 mm × 5 μm column) to provide the title compound as a white solid (24 mg, 58%). LC-MS (ESI) *m/z*: 346.0 (M + H)⁺; ¹H NMR (400 MHz, DMSO-*d*₆): δ 8.24 (s, 1H), 7.78 (s, 1H), 7.48 (s, 1H), 3.89 (s, 4H), 3.65 (br d, *J* = 10.8 Hz, 1H), 2.56 (br s, 1H), 2.22–2.11 (m, 1H), 2.04 (t, *J* = 11.9 Hz, 1H), 1.76 (br d, *J* = 13.1 Hz, 1H), 1.36 (br s, 1H), 0.76–0.64 (m, 1H), 0.62 (d, *J* = 6.8 Hz, 3H).

(3-{4-[(3R,5S)-3-Amino-5-methylpiperidin-1-yl]-6-chloro-7H-pyrrolo[2,3-d]pyrimidin-5-yl}phenyl)methanol (15). A flask was charged with [3-(4,6-dichloro-7-[[2-(trimethylsilyl)ethoxy]methyl]-7H-pyrrolo[2,3-d]pyrimidin-5-yl]phenyl)methanol (130 mg, 0.30 mmol), *tert*-butyl [(3R,5S)-5-methylpiperidin-3-yl]carbamate (69 mg, 0.32 mmol), acetonitrile (3 mL), and DIPEA (0.16 mL, 0.92 mmol). The reaction was heated to 65 °C for 20 h and then concentrated to provide a yellow gum. The crude material was purified using column chromatography (5:1 petroleum ether/ethyl acetate) to provide the title compound as a yellow gum (150 mg), which was carried on to the next step without further analysis. A flask was charged with the resulting material (150 mg), DCM (5 mL), and

trifluoroacetic acid (5 mL). The reaction was allowed to stir at 20 °C for 3 h. The solution was concentrated in vacuo, re-dissolved in THF (20 mL), and concentrated again. The residue was then dissolved in methanol, and the pH was adjusted to 9–10 by addition of concentrated ammonium hydroxide. The solution was stirred for 30 min and then purified using HPLC (29–59% acetonitrile in 0.05% v/v aqueous ammonium hydroxide, gradient time = 10 min, flow rate = 25 mL/min, Agela DuraShell C18, 150 mm × 25 mm × 5 μm column) to provide the title compound as a white solid (40 mg, 35%). LC–MS (ESI) *m/z*: 372.1 (M + H)⁺; ¹H NMR (400 MHz, DMSO-*d*₆): δ 8.34–8.27 (m, 1H), 7.84 (dd, *J* = 1.3, 6.5 Hz, 1H), 7.70 (br s, 1H), 3.91–3.80 (m, 1H), 3.61–3.54 (m, 1H), 2.45–2.38 (m, 1H), 2.35 (d, *J* = 2.0 Hz, 3H), 2.17 (dd, *J* = 10.7, 12.2 Hz, 1H), 2.06–1.95 (m, 1H), 1.76 (br d, *J* = 12.5 Hz, 1H), 1.10–0.92 (m, 1H), 0.69 (q, *J* = 12.0 Hz, 1H), 0.59 (d, *J* = 6.8 Hz, 3H).

3-[4-[(3*R*,5*S*)-3-Amino-5-methylpiperidin-1-yl]-6-chloro-7*H*-pyrrolo[2,3-*d*]pyrimidin-5-yl]-2-chlorobenzonitrile (17). A flask was charged with *tert*-butyl [(3*R*,5*S*)-1-(6-chloro-5-iodo-7-[[2-(trimethylsilyl)ethoxy]methyl]-7*H*-pyrrolo[2,3-*d*]pyrimidin-4-yl)-5-methylpiperidin-3-yl]carbamate **S19** (300 mg, 0.48 mmol), (2-chloro-3-cyanophenyl)boronic acid (114 mg, 0.62 mmol), 1,4-dioxane (10 mL), water (1 mL), tripotassium phosphate (307 mg, 1.45 mmol), and *bis*(*tri-tert*-butylphosphine)palladium(0) (25 mg, 0.048 mmol). The mixture was degassed and purged with nitrogen (3×). The reaction was heated to 80 °C for 24 h. The solution was concentrated in vacuo, and the resulting material was purified using column chromatography (3:1 petroleum ether/ethyl acetate) to provide a pale-yellow gum (100 mg), which was carried on to the next step without further analysis. A flask was charged with the isolated material (100 mg), DCM (5 mL), and trifluoroacetic acid (5 mL). The reaction was allowed to stir at 20 °C for 2 h. The solution was concentrated in vacuo, and the resulting residue was diluted with THF and concentrated again. The resulting material was diluted with methanol, and the pH was adjusted to 7–8 by addition of concentrated ammonium hydroxide. The crude material was isolated as a mixture of atropidiastereomers and was purified using HPLC (29–59% acetonitrile in 0.05% v/v aqueous ammonia hydroxide, gradient time = 10 min, flow rate = 25 mL/min, Agela DuraShell C18, 150 mm × 25 mm × 5 μm column) to provide the title compound as a white solid (15 mg, 8%). Notably, after separation and lyophilization, each atropisomer equilibrated to a mixture of atropidiastereomers. LC–MS (ESI) *m/z*: 400.9 (M + H)⁺; ¹H NMR (400 MHz, DMSO-*d*₆): δ 8.26 (d, *J* = 3.3 Hz, 1H), 8.02 (br d, *J* = 7.5 Hz, 1H), 7.87–7.53 (m, 2H), 3.98–3.84 (m, 1H), 3.36–3.24 (m, 1H), 2.34 (br s, 1H), 2.20 (br t, *J* = 11.4 Hz, 1H), 1.99–1.86 (m, 1H), 1.77–1.64 (m, 1H), 0.92–0.60 (m, 2H), 0.55–0.45 (m, 3H).

3-[4-[(3*R*)-3-Hydroxypiperidin-1-yl]-7-[[2-(trimethylsilyl)ethoxy]methyl]-7*H*-pyrrolo[2,3-*d*]pyrimidin-5-yl]benzonitrile (S22). A flask was charged with 3-(4-chloro-7-[[2-(trimethylsilyl)ethoxy]methyl]-7*H*-pyrrolo[2,3-*d*]pyrimidin-5-yl)benzonitrile²³ (100 mg, 0.26 mmol), (3*R*)-piperidin-3-ol (68 mg, 0.39 mmol), DMSO (4 mL), and DIPEA (0.27 mL, 1.56 mmol). The reaction was sealed, heated to 100 °C, and allowed to stir for 16 h. The reaction was diluted with water (15 mL) and extracted with ethyl acetate (2 × 10 mL). The combined organic layer was washed with brine (2 × 15 mL), dried over anhydrous sodium sulfate, filtered, and concentrated to provide a yellow gum, which was combined with the crude material from another reaction (60 mg). The combined crude material was purified using column chromatography (1:1 ethyl acetate/petroleum ether) to provide the title compound as a yellow gum (100 mg, 57% average yield). LC–MS (ESI) *m/z*: 450.3 (M + H)⁺; ¹H NMR (400 MHz, methanol-*d*₄): δ 8.41 (s, 1H), 7.90 (d, *J* = 1.5 Hz, 1H), 7.85 (td, *J* = 1.4, 7.7 Hz, 1H), 7.73–7.68 (m, 1H), 7.68–7.62 (m, 1H), 7.60 (s, 1H), 5.67 (s, 2H), 3.87–3.79 (m, 1H), 3.68–3.59 (m, 2H), 3.59–3.50 (m, 2H), 2.89–2.77 (m, 2H), 1.89 (br d, *J* = 3.5 Hz, 1H), 1.54 (br s, 1H), 1.41–1.27 (m, 2H), 0.95–0.86 (m, 2H), –0.03–0.10 (m, 9H).

3-[4-[(3*R*)-3-Hydroxypiperidin-1-yl]-7*H*-pyrrolo[2,3-*d*]pyrimidin-5-yl]benzonitrile (10). A flask was charged with 3-(4-[(3*R*)-3-hydroxypiperidin-1-yl]-7-[[2-(trimethylsilyl)ethoxy]methyl]-

7*H*-pyrrolo[2,3-*d*]pyrimidin-5-yl)benzonitrile **S22** (100 mg, 0.222 mmol) and DCM (3 mL). The solution was cooled to 0 °C, and trifluoroacetic acid (3 mL) was added. The reaction was allowed to warm to room temperature and was stirred for 3 h. The reaction was concentrated in vacuo, and the resulting residue was dissolved in 1,4-dioxane (3 mL) and 30–32% aqueous ammonium hydroxide (1 mL). The mixture was allowed to stir at room temperature for 30 min and then was concentrated in vacuo. The resulting material was diluted with water (15 mL) and extracted with ethyl acetate (5 × 15 mL). The combined organic layer was dried over anhydrous sodium sulfate, filtered, and concentrated to provide the title compound as a white solid (58.6 mg, 83%). LC–MS (ESI) *m/z*: 320.1 (M + H)⁺; ¹H NMR (400 MHz, methanol-*d*₄): δ 8.34 (s, 1H), 7.94–7.80 (m, 2H), 7.72–7.53 (m, 2H), 7.45 (s, 1H), 3.87–3.79 (m, 1H), 3.63–3.48 (m, 2H), 2.88–2.74 (m, 2H), 1.89 (br s, 1H), 1.61–1.47 (m, 1H), 1.36–1.24 (m, 2H).

3-(4-[(3*R*)-3-Aminopiperidin-1-yl]-6-chloro-7-[[2-(trimethylsilyl)ethoxy]methyl]-7*H*-pyrrolo[2,3-*d*]pyrimidin-5-yl)benzonitrile (S23). A flask was charged with 3-(4,6-dichloro-7-[[2-(trimethylsilyl)ethoxy]methyl]-7*H*-pyrrolo[2,3-*d*]pyrimidin-5-yl)benzonitrile **28** (192 mg, 0.458 mmol), *R*-3-Boc-aminopiperidine (92 mg, 0.458 mmol), and acetonitrile (2.3 mL). DIPEA (0.38 mL, 2.3 mmol) was added, and the reaction was heated to 80 °C (MW) for 1 h. The reaction was concentrated. The crude material was purified using column chromatography (0–100% ethyl acetate in heptane) to provide the title compound (329 mg, 99%). ¹H NMR (400 MHz, CDCl₃): δ 8.52 (s, 1H) 7.82 (s, 1H) 7.66–7.75 (m, 2H) 7.52–7.65 (m, 1H) 5.75 (d, *J* = 1.47 Hz, 2H) 4.99–5.13 (m, 1H) 3.67–3.75 (m, 2H) 3.48–3.64 (m, 2H) 3.05–3.24 (m, 2H) 2.75–2.97 (m, 1H) 1.69–1.81 (m, 1H) 1.27–1.33 (m, 1H) 1.08–1.20 (m, 1H) 1.00 (dd, *J* = 8.93, 7.58 Hz, 2H) –0.09–0.08 (m, 9H).

3-[4-[(3*R*)-3-Aminopiperidin-1-yl]-6-chloro-7*H*-pyrrolo[2,3-*d*]pyrimidin-5-yl]benzonitrile (8). A flask was charged with 3-(4-[(3*R*)-3-aminopiperidin-1-yl]-6-chloro-7-[[2-(trimethylsilyl)ethoxy]methyl]-7*H*-pyrrolo[2,3-*d*]pyrimidin-5-yl)benzonitrile (268 mg, 0.460 mmol) and DCM (3 mL). Trifluoroacetic acid (2 mL) was added at 30 °C, and the reaction was allowed to stir overnight. The mixture was concentrated in vacuo to provide a yellow oil, which was diluted with methanol (6 mL). Potassium carbonate (318 mg, 2.30 mmol) was added, and the mixture was allowed to stir for 3 h. The material was concentrated in vacuo, and the resulting material was stirred with DCM, filtered, and concentrated in vacuo. The crude material was purified using HPLC to provide the title compound (53.2 mg, 33%). ¹H NMR (400 MHz, DMSO-*d*₆): δ 8.22 (s, 1H) 7.67–7.77 (m, 3H) 7.59 (d, *J* = 7.83 Hz, 1H) 3.57–3.70 (m, 1H) 3.29–3.32 (m, 2H) 2.20–2.37 (m, 3H) 1.55–1.68 (m, 1H) 1.14–1.28 (m, 1H) 0.84–1.05 (m, 2H).

Co-Crystal Structures. The cocrystal structures described here have been deposited in the Protein Data Bank (wwPDB), and the details of the methods used can be found under accession codes 8FH4 (HPK1 + compound **2**, 1.83 Å), 8FP1 (PKCη + compound **2**, 1.75 Å), 8FJZ (HPK1 + compound **11**, 1.90 Å), 8FP3 (PKCη + compound **11**, 1.95 Å), and 8FKO (HPK1 + compound **19**, 2.10 Å). Authors will release the atomic coordinates upon article publication. HPK1-inhibitor complexes were obtained from the 1–307; T165E, S171E construct¹⁵ and were crystallized by the sitting drop vapor diffusion method at 13 °C. Crystals were grown by mixing purified protein (15 mg/mL)–inhibitor (0.001 M) complex solution with a crystallization solution containing 18–20% 1,6-hexanediol, 0.1 M tris at pH 8.0, 0.01 M magnesium sulfate, and 0.02–0.04 M barium acetate. The drops were set up at a protein to crystallization solution ratio of 1:1.5. PKCη-inhibitor complexes were obtained from the 333–683; S675E construct via soaking of apo crystals. Apo crystals were grown using the sitting drop vapor diffusion method at 13 °C by mixing purified protein solution (12 mg/mL) with a crystallization solution containing 21–23% (w/v) poly(ethylene glycol) (MW 3350), 0.7 M lithium nitrate, 7% (w/v) glycerol, and 0.1 M MES buffer at pH 6.0. The crystallization drops were set up at a protein to crystallization solution ratio of 1:1.6. Crystal soaks were performed by saturating crystallization drops containing preformed crystals with a

soaking solution containing inhibitor (0.01 M), 38% (w/v) poly(ethylene glycol) (MW 3350), 0.7 M lithium nitrate, 10% (w/v) glycerol, and 0.1 M MES buffer at pH 6.0. Drops were sealed and incubated at 13 °C for 60–120 min prior to crystal harvest. Crystals were flash-frozen in liquid N₂, and X-ray diffraction data were collected at the Advanced Photon Source beamline 17-ID at Argonne National Labs. Diffraction data were processed with autoPROC from Global Phasing,²⁷ and structure solution and model refinement were done using BUSTER,²⁸ and COOT.²⁹ The HPK1-inhibitor complex structures were solved using the previously reported HPK1-Sutent structure,¹⁵ and the PKC η -inhibitor complexes were initially solved using the crystal structure of PKC- θ as the starting model,³⁰ PDB 1XJD.

Homology Model Generation. A homology model of HPK1 was created through a chimeric approach by selection of various sections of multiple kinase proteins. A DFG-in homology model of HPK1 was constructed from MST1, which was the closest protein kinase with an available structure (KD similarity 46% and ATP binding pocket similarity 78%). The MST1 structure selected had a disordered G-loop so a structure of ABL, which had identical G-loop sequence identity to HPK1; it was the template for the homology model of the HPK1 G-loop. Additionally, the conformation of Met91 was analyzed relative to other kinases with a methionine gatekeeper. The conformation of Met91 in the HPK1 homology model was adjusted to be in line with the most commonly observed conformations across the kinome.

Virtual Screening Paradigm. A relevant set of compounds for screening were selected by leveraging legacy data on an in-house collection of 1.8 million compounds. A subset of these compounds was prioritized for virtual screening in the homology model (LigandScout and Glide docking) based on confidence that they would be active (activity against a structurally similar kinase) and selective (low promiscuity based on all available kinase data). Overall, 1864 compounds were selected to be tested based on this paradigm. Out of this number, 63 molecules over 15 chemotypes were identified as highly active hits.

Biochemical Assays for HPK1, PKC θ , and PKC η .²⁹ Inhibition of human full-length recombinant HPK1, PKC θ , and PKC η enzymes was measured using a microfluidic mobility-shift assay at Pfizer Inc., San Diego. The reactions were conducted in 50 μ L volumes in 96-well plates. Compounds were tested in 11-dose 3-fold serial dilutions (2% DMSO final or DMSO only). Non-tagged HPK1 protein was produced at Pfizer Inc. by expression in baculovirus-infected insect cells and activated by autophosphorylation with MgATP. PKC θ was purchased from Invitrogen (C-terminal hexahistidine-tagged); no special measures were taken to activate this kinase. Non-tagged PKC η was prepared at Pfizer Inc. by expression in baculovirus-infected insect cells; no special measures were taken to activate this kinase. HPK1 assays contained 0.5 nM HPK1, 3 μ M phosphoacceptor peptide (5-FAM-AKRRRLSSLRA-COOH, CPC Scientific, Sunnyvale, CA), 1 mM DTT, 0.002% Tween-20, and 2.5 mM MgCl₂ in 50 mM MOPS, pH 7.8. Reactions were initiated by addition of 75 μ M adenosine 5'-triphosphate (ATP), following a 20 min preincubation. The reactions were incubated for 1 h at 37 °C. Reactions were stopped by the addition of 50 μ L 0.015 M EDTA, pH 8, and the extent of reactions (~15–20% conversion with no inhibitor) was determined after electrophoretic separation of the fluorescently labeled peptide substrate and phosphorylated product on a LabChip EZ Reader II (PerkinElmer, Inc., Waltham, MA). The K_i values were calculated by fitting the % conversion to the Morrison equation for tight-binding competitive inhibition³¹ using ABase software (IDBS, London, United Kingdom) and experimentally measured apparent Michaelis constant of MgATP ($K_m = 29 \mu$ M) for HPK1. PKC θ and PKC η assays contained 0.02 nM PKC θ or 0.2 nM PKC η , 3 μ M phosphoacceptor peptide (5-FAM-RFARKGSLRQKNV-COOH, CPC Scientific, Sunnyvale, CA), 1 mM DTT, 10 μ g/mL 3-*sn*-phosphatidyl-L-serine sodium salt, 3.6 μ g/mL 1,2-dioleoyl-*sn*-glycerol, 0.01% Brij-35, and 12.5 mM MgCl₂ in 50 mM HEPES, pH 7.5. Reactions were initiated by addition of ATP following a 20 min preincubation and were performed at a K_m concentration of MgATP

(PKC θ $K_m = 120 \mu$ M, PKC η $K_m = 31 \mu$ M). The reactions were incubated for 1 h for PKC θ and 30 min for PKC η at a controlled RT. Reactions were stopped and analyzed in the same way as HPK1. For all biochemical activities reported, values reported are geometric means \pm arithmetic standard deviation where $n \geq 3$ repeats were completed in the assay, unless otherwise noted.

Kinase Selectivity Panel Assays. Biochemical profiling (73 wild-type kinase assays) was conducted using Thermo Fisher Scientific, Inc. Invitrogen SelectScreen screening service in their Madison, WI, facility. Most of the kinase panel assays were the fluorescence resonance energy transfer (FRET)-based Z'-LYTE assays that employed a fluorescence-based, coupled-enzyme format, taking advantage of the differential sensitivity of phosphorylated and nonphosphorylated peptides to proteolytic cleavage. Two other formats of Invitrogen assays were the time-resolved fluorescence resonance energy transfer (TR-FRET)-based Adapta technology, which employs an Alexa Fluor 647-labeled adenosine diphosphate (ADP) tracer and Eu-labeled anti-ADP antibody, and the TR-FRET-based LanthaScreen binding assay, utilizing an Alexa Fluor ATP site targeted tracer and Eu-labeled anti-tag antibody that binds to the respective affinity tag of the target kinase. All Z'-LYTE or Adapta kinase assays were conducted at a K_m concentration of MgATP, except for RAF1 Y340D, Y341D (a "cascade" Z'-LYTE assay with 100 μ M MgATP). LanthaScreen competition binding assays were performed with the Alexa Fluor ATP site tracer present at a dissociation constant (K_D) level (with no ATP added). Percent (%) inhibition for each kinase was measured with respect to DMSO control and reported as an average of duplicate measurements. Each IC₅₀ determination was based on 10-dose duplicate measurements, fitted to a standard four-parameter IC₅₀ equation.

Phospho-SLP-76 (Ser376) HTRF Assay. Jurkat cells were seeded at 90,000 cells/well in 90 μ L of RPMI1640 growth medium containing 10% FBS and incubated at 37 °C with 5% CO₂ overnight. The following day, compounds were serially diluted in DMSO and added to cells for final concentration 10 μ M to 0.1 nM in 0.1% DMSO. After 30 min pre-treatment with compounds, the cells were stimulated using 200 μ g/mL of F(ab)2 complexed anti-CD3 (clone UCTH1) for 15 min at 37 °C with 5% carbon dioxide. Stimulation was stopped with ice cold PBS, and cells were harvested by centrifugation before lysis in Cisbio lysis buffer (Cisbio, Bedford, MA). Lysates were incubated overnight with anti-phospho-SLP-76-*cryptate* plus anti-phospho-SLP-76-d2 homogeneous time-resolved fluorescence (HTRF) antibodies at room temperature protected from light according to the manufacturer's protocol (Cisbio, Bedford, MA). HTRF was measured on a PerkinElmer Envision, and IC₅₀ values were calculated by concentration–response curve fitting utilizing four-parameter nonlinear regression analyses. Values reported are geometric means \pm standard deviation, where $n \geq 3$ repeats were completed in the assay unless otherwise noted within the table.

Cell-Based IL-2 Assay. Jurkat WT and HPK1-/- cells were seeded at 200 K/well in 96-well U bottom plates in 180 μ L of RPMI growth media (RPMI + 10% FBS, 1% glutamax and 1% PenStrep). After seeding, cells were allowed to rest for 30 min at 37 °C. Compounds were serial-diluted (1:3) in DMSO and further diluted to 10 \times in RPMI media containing no supplements. Compounds were added to cells (1 \times) and incubated for 30 min at 37 °C. Cells were stimulated with 1 M Dynal Human T-Activator CD3/CD28 Dynabeads/well (Gibco Cat no. 11131D) and were incubated for 24 h at 37 °C. Cell supernatants were collected after 24 h, and IL-2 levels (pg/mL) were measured by using a Human IL-2 Quantikine ELISA kit (R&D Systems Cat no. D2050). The manufacturer's protocol was altered slightly to optimize assay results. The alterations include an overnight cell supernatant incubation at 4 °C and a 3 h incubation following IL-2 conjugate addition. The IL-2 response was determined by the fold enhancement between compound treatments and stimulated-only controls. The EC₅₀ values were calculated in GraphPad Prism 7.04 using a four-parameter dose response stimulation curve [log (agonist) vs response–variable slope]. Values reported are geometric means \pm standard deviation, where $n \geq 3$ repeats were completed in the assay.

SF Log D Assay. Shake flask log *D* (SF log *D*) is the log of the octanol/water ratio measured using the shake-flask method.³²

■ ASSOCIATED CONTENT

SI Supporting Information

The Supporting Information is available free of charge at <https://pubs.acs.org/doi/10.1021/acs.jmedchem.2c02038>.

Canonical smiles and biological data summary (CSV)
X-ray data; NMR studies with compound **19**; kinase selectivity data for compound **1**, **2**, and **18**; and Pliers scoring for compound **2** (PDF)

■ AUTHOR INFORMATION

Corresponding Authors

Rebecca A. Gallego – Oncology Medicinal Chemistry, Pfizer Worldwide Research and Development, La Jolla, California 92121, United States; orcid.org/0000-0001-7893-9032; Phone: (858)-622-7319; Email: rebecca.gallego@pfizer.com

Sajiv K. Nair – Oncology Medicinal Chemistry, Pfizer Worldwide Research and Development, La Jolla, California 92121, United States; orcid.org/0000-0002-8628-6999; Phone: (858)-526-4894; Email: sajiv.k.nair@pfizer.com

Authors

Louise Bernier – Oncology Medicinal Chemistry, Pfizer Worldwide Research and Development, La Jolla, California 92121, United States

Hui Chen – WuXi AppTec, Shanghai 200131, China

Sujin Cho-Schultz – Oncology Medicinal Chemistry, Pfizer Worldwide Research and Development, La Jolla, California 92121, United States

Loanne Chung – Oncology Medicinal Chemistry, Pfizer Worldwide Research and Development, La Jolla, California 92121, United States

Michael Collins – Oncology Medicinal Chemistry, Pfizer Worldwide Research and Development, La Jolla, California 92121, United States

Matthew Del Bel – Oncology Medicinal Chemistry, Pfizer Worldwide Research and Development, La Jolla, California 92121, United States

Jeff Elleraas – Oncology Medicinal Chemistry, Pfizer Worldwide Research and Development, La Jolla, California 92121, United States

Cinthia Costa Jones – Oncology Research Unit, Pfizer Worldwide Research and Development, La Jolla, California 92121, United States

Ciaran N. Cronin – Oncology Medicinal Chemistry, Pfizer Worldwide Research and Development, La Jolla, California 92121, United States

Martin Edwards – Oncology Medicinal Chemistry, Pfizer Worldwide Research and Development, La Jolla, California 92121, United States

Xu Fang – WuXi AppTec, Shanghai 200131, China

Timothy Fisher – Oncology Research Unit, Pfizer Worldwide Research and Development, La Jolla, California 92121, United States

Mingying He – Oncology Medicinal Chemistry, Pfizer Worldwide Research and Development, La Jolla, California 92121, United States

Jacqui Hoffman – Oncology Medicinal Chemistry, Pfizer Worldwide Research and Development, La Jolla, California 92121, United States

Ruiduan Huo – WuXi AppTec, Shanghai 200131, China
Mehran Jalaie – Oncology Medicinal Chemistry, Pfizer Worldwide Research and Development, La Jolla, California 92121, United States

Eric Johnson – Oncology Medicinal Chemistry, Pfizer Worldwide Research and Development, La Jolla, California 92121, United States

Ted W. Johnson – Oncology Medicinal Chemistry, Pfizer Worldwide Research and Development, La Jolla, California 92121, United States; orcid.org/0000-0002-3541-9747

Robert S. Kania – Oncology Medicinal Chemistry, Pfizer Worldwide Research and Development, La Jolla, California 92121, United States

Manfred Kraus – Oncology Research Unit, Pfizer Worldwide Research and Development, La Jolla, California 92121, United States

Jennifer Lafontaine – Oncology Medicinal Chemistry, Pfizer Worldwide Research and Development, La Jolla, California 92121, United States

Puong Le – Oncology Medicinal Chemistry, Pfizer Worldwide Research and Development, La Jolla, California 92121, United States

Tongnan Liu – WuXi AppTec, Shanghai 200131, China

Michael Maestre – La Jolla Laboratories, Pfizer Worldwide Research and Development, La Jolla, California 92121, United States

Jean Matthews – Oncology Medicinal Chemistry, Pfizer Worldwide Research and Development, La Jolla, California 92121, United States

Michele McTigue – Oncology Medicinal Chemistry, Pfizer Worldwide Research and Development, La Jolla, California 92121, United States

Nichol Miller – Oncology Research Unit, Pfizer Worldwide Research and Development, La Jolla, California 92121, United States

Qiming Mu – WuXi AppTec, Shanghai 200131, China

Xulong Qin – WuXi AppTec, Shanghai 200131, China

Shijian Ren – WuXi AppTec, Shanghai 200131, China

Paul Richardson – Oncology Medicinal Chemistry, Pfizer Worldwide Research and Development, La Jolla, California 92121, United States; orcid.org/0000-0002-3700-8749

Allison Rohner – Oncology Research Unit, Pfizer Worldwide Research and Development, La Jolla, California 92121, United States

Neal Sach – Oncology Medicinal Chemistry, Pfizer Worldwide Research and Development, La Jolla, California 92121, United States

Li Shao – WuXi AppTec, Shanghai 200131, China

Graham Smith – Oncology Medicinal Chemistry, Pfizer Worldwide Research and Development, La Jolla, California 92121, United States

Ruirui Su – WuXi AppTec, Shanghai 200131, China

Bin Sun – WuXi AppTec, Shanghai 200131, China

Sergei Timofeevski – Oncology Research Unit, Pfizer Worldwide Research and Development, La Jolla, California 92121, United States

Puong Tran – Oncology Medicinal Chemistry, Pfizer Worldwide Research and Development, La Jolla, California 92121, United States

Shuiwang Wang – WuXi AppTec, Shanghai 200131, China

Wei Wang – Oncology Medicinal Chemistry, Pfizer Worldwide Research and Development, La Jolla, California 92121, United States; orcid.org/0000-0003-2611-8210

Ru Zhou – Oncology Medicinal Chemistry, Pfizer Worldwide Research and Development, La Jolla, California 92121, United States

Jinjiang Zhu – Oncology Medicinal Chemistry, Pfizer Worldwide Research and Development, La Jolla, California 92121, United States

Complete contact information is available at:

<https://pubs.acs.org/10.1021/acs.jmedchem.2c02038>

Notes

The authors declare the following competing financial interest(s): The authors with Pfizer affiliation are employees and shareholders of Pfizer.

ACKNOWLEDGMENTS

The authors are grateful to Steven Burakoff and Sansana Sawasdikol for supplying Jurkat HPK1 KO cells, and Wei Liu for providing PKC η for co-crystal structures.

ABBREVIATIONS

APCI, atmospheric pressure chemical ionization; Boc, *tert*-butyloxycarbonyl; DCM, dichloromethane; DIPEA, diisopropylethylamine; DMF, dimethylformamide; DMSO, dimethylsulfoxide; ES, electrostatics; ESI, electrospray ionization; HPK1, hematopoietic progenitor kinase-1; HPLC, high-performance liquid chromatography; KO, knock out; LCMS, liquid chromatography–mass spectrometry; LiHMDS, lithium hexamethyldisilazide; LipE, lipophilic efficiency; LS, local ligand strain energy; MAD, median absolute deviation; MAP4K1, mitogen-activated protein kinase kinase kinase 1; MAP4K2, mitogen-activated protein kinase kinase kinase 2; MAP4K3, mitogen-activated protein kinase kinase kinase 3; MAP4K5, mitogen-activated protein kinase kinase kinase 5; MST1, mammalian STE20-like protein kinase 1; MST2, mammalian STE20-like protein kinase 2; MST3, mammalian STE20-like protein kinase 3; MST4, mammalian STE20-like protein kinase 4; ND, not determined; NIS, *N*-chlorosuccinimide; NIS, *N*-iodosuccinimide; PBMC, peripheral blood mononuclear cell; PKC θ , protein kinase C, theta; PS, protein strain energy; SBDD, structure-based drug design; SEM, 2-(trimethylsilyl)ethoxymethyl; SEMCl, 2-(trimethylsilyl)ethoxymethyl chloride; SF log *D*, shake-flask log *D*; SLP76, SH2 domain containing leukocyte protein of 76 kDa; SnAr, nucleophilic aromatic substitution; SFC, supercritical fluid chromatography; TBHP, *tert*-butyl hydrogen peroxide; TFA, trifluoroacetic acid; THF, tetrahydrofuran; TLC, thin-layer chromatography; VdW, van der Waals; WT, wildtype

REFERENCES

- (1) Chuang, H. C.; Wang, X.; Tan, T. H. MAP4K Family Kinases in Immunity and Inflammation. *Adv. Immunol.* **2016**, *129*, 277–314.
- (2) Sawasdikol, S.; Zha, R.; Yang, B.; Burakoff, S. HPK1 as a novel target for cancer immunotherapy. *Immunol. Res.* **2012**, *54*, 262.
- (3) Alzabin, S.; Pyarajan, S.; Yee, H.; Kiefer, F.; Suzuki, A.; Burakoff, S.; Sawasdikol, S. Hematopoietic progenitor kinase 1 is a critical component of prostaglandin E2-mediated suppression of the anti-tumor immune response. *Cancer Immunol. Immunother.* **2010**, *59*, 419–429.
- (4) Liou, J.; Kiefer, F.; Dang, A.; Hashimoto, A.; Cobb, M. H.; Kurosaki, T.; Weiss, A. HPK1 is activated by lymphocyte antigen receptors and negatively regulates AP-1. *Immunity* **2000**, *12*, 399–408.

- (5) Sauer, K.; Liou, J.; Singh, S. B.; Yablonski, D.; Weiss, A.; Perlmutter, R. M. Hematopoietic progenitor kinase 1 associates physically and functionally with the adaptor proteins B cell linker protein and SLP-76 in lymphocytes. *J. Biol. Chem.* **2001**, *276*, 45207–45216.

- (6) Bartolo, V.; Montagne, B.; Salek, M.; Jungwirth, B.; Carrette, F.; Fourtane, J.; Sol-Foulon, N.; Michel, F.; Schwartz, O.; Lehmann, W. D.; Acuto, O. A novel pathway down-modulating T cell activation involves HPK-1-dependent recruitment of 14-3-3 proteins on SLP-76. *J. Exp. Med.* **2007**, *204*, 681–691.

- (7) Navas, V. H.; Cuche, C.; Alcover, A.; Di Bartolo, V. Serine Phosphorylation of SLP76 Is Dispensable for T Cell Development but Modulates Helper T Cell Function. *PLoS One* **2017**, *12*, No. e0170396.

- (8) Alzabin, S.; Bhardwaj, N.; Kiefer, F.; Sawasdikol, S.; Burakoff, S. Hematopoietic progenitor kinase 1 is a negative regulator of dendritic cell activation. *J. Immunol.* **2009**, *182*, 6187–6194.

- (9) Shui, J. W.; Boomer, J. S.; Han, J.; Xu, J.; Dement, G. A.; Zhou, G.; Tan, T. H. Hematopoietic progenitor kinase 1 negatively regulates T cell receptor signaling and T cell-mediated immune responses. *Nat. Immunol.* **2007**, *8*, 84–91.

- (10) Liu, J.; Curtin, J.; You, D.; Hillerman, S.; Li-Wang, B.; Eraslan, R.; Xie, J.; Swanson, J.; Ho, C. P.; Oppenheimer, S.; Warrack, B. M.; McNaney, C. A.; Nelson, D. M.; Blum, J.; Kim, T.; Fereshteh, M.; Reily, M.; Shipkova, P.; Murtaza, A.; Sanjuan, M.; Hunt, J. T.; Salter-Cid, L. Critical role of kinase activity of hematopoietic progenitor kinase 1 in anti-tumor immune surveillance. *PLoS One* **2019**, *14*, No. e0212670.

- (11) Hernandez, S.; Qing, J.; Thibodeau, R. H.; Du, X.; Park, S.; Lee, H. M.; Xu, M.; Oh, S.; Navarro, A.; Roose-Girma, M.; Newman, R. J.; Warming, S.; Nannini, M.; Sampath, D.; Kim, J. M.; Grogan, J. L.; Mellman, I. The Kinase Activity of Hematopoietic Progenitor Kinase 1 Is Essential for the Regulation of T Cell Function. *Cell Rep.* **2018**, *25*, 80–94.

- (12) Davis, M. I.; Hunt, J. P.; Herrgard, S.; Ciceri, P.; Wodicka, L. M.; Pallares, G.; Hocker, M.; Treiber, D. K.; Zarrinkar, P. P. Comprehensive analysis of kinase inhibitor selectivity. *Nat. Biotechnol.* **2011**, *29*, 1046–1051.

- (13) Zhu, Q.; Chen, N.; Tian, X.; Zhou, Y.; You, Q.; Xu, X. Hematopoietic Progenitor Kinase 1 in Tumor Immunology: A Medicinal Chemistry Perspective. *J. Med. Chem.* **2022**, *65*, 8065–8090.

- (14) Altman, A.; Isakov, N.; Baier, G. Protein kinase C θ : a new essential superstar on the T-cell stage. *Immunol. Today* **2000**, *21*, 567–573.

- (15) Johnson, E.; McTigue, M.; Gallego, R. A.; Johnson, T. W.; Timofeevski, S.; Maestre, M.; Fisher, T. S.; Kania, R.; Sawasdikol, S.; Burakoff, S.; Cronin, C. N. Multiple conformational states of the HPK1 kinase domain in complex with sunitinib reveal the structural changes accompanying HPK1 trans-regulation. *J. Biol. Chem.* **2019**, *294*, 9029.

- (16) Johnson, T. W.; Gallego, R. A.; Edwards, M. P. Lipophilic Efficiency as an Important Metric in Drug Design. *J. Med. Chem.* **2018**, *61*, 6401–6420.

- (17) Milletti, F.; Storchi, L.; Sforna, G.; Cruciani, G. New and original pKa prediction method using grid molecular interaction fields. *J. Chem. Inf. Model.* **2007**, *47*, 2172–2181.

- (18) Milletti, F.; Storchi, L.; Sforna, G.; Cross, S.; Cruciani, G. Tautomer enumeration and stability prediction for virtual screening on large chemical databases. *J. Chem. Inf. Model.* **2009**, *49*, 68–75.

- (19) Milletti, F.; Vulpetti, A. Tautomer preference in PDB complexes and its impact on structure-based drug discovery. *J. Chem. Inf. Model.* **2010**, *50*, 1062–1074.

- (20) Di, L.; Whitney-Pickett, C.; Umland, J. P.; Zhang, H.; Zhang, X.; Gebhard, D. F.; Lai, Y.; Federico, J. J.; Davidson, R. E.; Smith, R.; Reyner, E. L.; Lee, C.; Feng, B.; Rotter, C.; Varma, M. V.; Kempshall, S.; Fenner, K.; El-kattan, A. F.; Liston, T. E.; Troutman, M. D. Development of a new permeability assay using low-efflux MDCKII cells. *J. Pharm. Sci.* **2011**, *100*, 4974–4985.

(21) Johnson, T. W.; Bolanos, B.; Brooun, A.; Gallego, R. A.; Gehlhaar, D.; Jalaie, M.; McTigue, M.; Timofeevski, S. Reviving B-Factors: Activating ALK Mutations Increase Protein Dynamics of the Unphosphorylated Kinase. *ACS Med. Chem. Lett.* **2018**, *9*, 872–877.

(22) Johnson, T. W.; Gallego, R. A.; Brooun, A.; Gehlhaar, D.; McTigue, M. Reviving B-Factors: Retrospective Normalized B-Factor Analysis of c-ros Oncogene 1 Receptor Tyrosine Kinase and Anaplastic Lymphoma Kinase L1196M with Crizotinib and Lorlatinib. *ACS Med. Chem. Lett.* **2018**, *9*, 878–883.

(23) Henderson, J. L.; Kormos, B. L.; Hayward, M. M.; Coffman, K. J.; Jasti, J.; Kurumbail, R. G.; Wager, T. T.; Verhoest, P. R.; Noell, G. S.; Chen, Y.; Needle, E.; Berger, Z.; Steyn, S. J.; Houle, C.; Hirst, W. D.; Galatsis, P. Discovery and preclinical profiling of 3-[4-(morpholin-4-yl)-7H-pyrrolo[2,3-d]pyrimidin-5-yl]benzotrile (PF-06447475), a highly potent, selective, brain penetrant, and in vivo active LRRK2 kinase inhibitor. *J. Med. Chem.* **2015**, *58*, 419–432.

(24) Medina, J. R.; Becker, C. J.; Blackledge, C. W.; Duquenne, C.; Feng, Y.; Grant, S. W.; Heerding, D.; Li, W. H.; Miller, W. H.; Romeril, S. P.; Scherzer, D.; Shu, A.; Bobko, M. A.; Chadderton, A. R.; Dumble, M.; Gardiner, C. M.; Gilbert, S.; Liu, Q.; Rabindran, S. K.; Sudakin, V.; Xiang, H.; Brady, P. G.; Campobasso, N.; Ward, P.; Axten, J. M. Structure-based design of potent and selective 3-phosphoinositide-dependent kinase-1 (PDK1) inhibitors. *J. Med. Chem.* **2011**, *54*, 1871–1895.

(25) Murphy, R. A.; Chen, A. Y.; Nair, S. K.; Gallego, G. M.; Sach, N. W.; Smith, G. Diastereoselective access to substituted 4-aminopiperidines via a pyridine reduction approach. *Tetrahedron Lett.* **2016**, *57*, 5588–5591.

(26) Gottlieb, H. E.; Kotlyar, V.; Nudelman, A. NMR Chemical Shifts of Common Laboratory Solvents as Trace Impurities. *J. Org. Chem.* **1997**, *62*, 7512–7515.

(27) Vonrhein, C.; Flensburg, C.; Keller, P.; Sharff, A.; Smart, O.; Paciorek, W.; Womack, T.; Bricogne, G. Data processing and analysis with the autoPROC toolbox. *Acta Crystallogr., Sect. D: Biol. Crystallogr.* **2011**, *67*, 293–302.

(28) Bricogne, G.; Blanc, E.; Brandl, M.; Flensburg, C.; Keller, P.; Paciorek, W.; Roversi, P.; Sharff, A.; Smart, O.; Vonrhein, C. *BUSTER Version 2.11. 2*; Global Phasing Ltd: Cambridge, United Kingdom, 2011.

(29) Emsley, P.; Cowtan, K. Coot: model-building tools for molecular graphics. *Acta Crystallogr., Sect. D* **2004**, *60*, 2126–2132.

(30) Xu, Z.-B.; Chaudhary, D.; Olland, S.; Wolfrom, S.; Czerwinski, R.; Malakian, K.; Lin, L.; Stahl, M. L.; Joseph-McCarthy, D.; Benander, C.; Fitz, L.; Greco, R.; Somers, W. S.; Mosyak, L. Catalytic Domain Crystal Structure of Protein Kinase C- θ (PKC θ). *J. Biol. Chem.* **2004**, *279*, 50401–50409.

(31) Morrison, J. F. Kinetics of the reversible inhibition of enzyme-catalysed reactions by tight-binding inhibitors. *Biochim. Biophys. Acta* **1969**, *185*, 269–286.

(32) Wilson, D. M.; Wang, X.; Walsh, E.; Rourick, R. A. High throughput log D determination using liquid chromatography-mass spectrometry. *Comb. Chem. High Throughput Screening* **2001**, *4*, 511–519.

Recommended by ACS

Design and Structural Optimization of Methionine Adenosyltransferase 2A (MAT2A) Inhibitors with High In Vivo Potency and Oral Bioavailability

Silong Zhang, Huan He, *et al.*

MARCH 24, 2023
JOURNAL OF MEDICINAL CHEMISTRY

READ 

Discovery of an *In Vivo* Chemical Probe for BCL6 Inhibition by Optimization of Tricyclic Quinolinones

Alice C. Harnden, Swen Hoelder, *et al.*

APRIL 07, 2023
JOURNAL OF MEDICINAL CHEMISTRY

READ 

BAY-6096: A Potent, Selective, and Highly Water-Soluble Adrenergic α_{2B} Antagonist

Daniel Meibom, Frank Wunder, *et al.*

MARCH 18, 2023
JOURNAL OF MEDICINAL CHEMISTRY

READ 

Modulation of ERK5 Activity as a Therapeutic Anti-Cancer Strategy

Duncan C. Miller, Celine Cano, *et al.*

APRIL 01, 2023
JOURNAL OF MEDICINAL CHEMISTRY

READ 

Get More Suggestions >